Tubulin tyrosination regulates synaptic function and is disrupted in Alzheimer's disease

Leticia Peris,[1,†,‡] Julie Parato,[2,3,†] Xiaoyi Qu,[2,†,§] Jean-Marc Soleilhac,[1] Fabien Lanté,[1] Atul Kumar,[2] Maria Elena Pero,[2,4] José Martínez-Hernández,[1,#] Charlotte Corrao,[1] Giulia Falivelli,[1] Floriane Payet,[1] Sylvie Gory-Fauré,[1] Christophe Bosc,[1] Marian Blanca Ramírez,[2] Andrew Sproul,[2] Jacques Brocard,[1] Benjamin Di Cara,[5] Philippe Delagrange,[5] Alain Buisson,[1] Yves Goldberg,[1] Marie-Jo Moutin,[1,‡] Francesca Bartolini[2,‡] and Annie Andrieux[1,‡]

1 Univ. Grenoble Alpes, Inserm, U1216, CEA, CNRS, Grenoble Institut Neurosciences, 38000 Grenoble, France

2 Department of Pathology & Cell Biology, Columbia University Irving Medical Center, New York, NY 10032, USA

3 Department of Natural Sciences, SUNY ESC, 177 Livingston St 6th Floor, Brooklyn, NY 11201, USA

4 Department of Veterinary Medicine and Animal Production, University of Naples Federico II, 80137, Naples, Italy

5 Institut de Recherche Servier, Croissy, France

[§]Present address: Genentech, San Francisco, CA 94080, USA

[#]Present address: Synaptic Structure Laboratory, Dept. Ciencias Médicas, Instituto de Investigación en Discapacidades Neurológicas (IDINE), Facultad de Medicina, Universidad Castilla-La Mancha, 02008 Albacete, Spain

Correspondence to: Leticia Peris

Grenoble Institut Neurosciences, Site santé La Tronche, BP170, 38042 Grenoble, France

E-mail: leticia.peris@univ-grenoble-alpes.fr

Correspondence may also be addressed to: Francesca Bartolini

Department of Pathology & Cell Biology, Columbia University Irving Medical Center, 630 W. 168(th) Street, New York, NY 10032, USA

E-mail: fb2131@cumc.columbia.edu

Running title: Tubulin tyrosination in Alzheimer's disease

[†,‡]These authors contributed equally to this work.

Abstract

Microtubules play fundamental roles in the maintenance of neuronal processes and in synaptic function and plasticity. While dynamic microtubules are mainly composed of tyrosinated tubulin, long-lived microtubules contain detyrosinated tubulin, suggesting that the tubulin tyrosination/detyrosination cycle is a key player in the maintenance of microtubule dynamics and neuronal homeostasis, conditions which go awry in neurodegenerative diseases. In the tyrosination/detyrosination cycle, the C-terminal tyrosine of α-tubulin is removed by tubulin carboxypeptidases and re-added by tubulin tyrosine ligase. Here we show that tubulin tyrosine ligase hemizygous mice exhibit decreased tyrosinated microtubules, reduced dendritic spine density, and both synaptic plasticity and memory deficits. We further report decreased tubulin tyrosine ligase expression in sporadic and familial Alzheimer's disease, and reduced microtubule dynamics in human neurons harboring the familial APP-V717I mutation. Finally, we show that synapses visited by dynamic microtubules are more resistant to oligomeric amyloid β peptide toxicity and that expression of tubulin tyrosine ligase, by restoring microtubule entry into spines, suppresses the loss of synapses induced by amyloid β peptide. Together, our results demonstrate that a balanced tyrosination/detyrosination tubulin cycle is necessary for the maintenance of synaptic plasticity, is protective against amyloid β peptide-induced synaptic damage, and that this balance is lost in Alzheimer's disease, providing evidence that defective tubulin retyrosination may contribute to circuit dysfunction during neurodegeneration in Alzheimer's disease.

Keywords: tubulin; microtubule; neuron; Alzheimer's disease; dendritic spines

Abbreviations: APP = Amyloid Precursor Protein; oAβ = oligomeric Amyloid β peptide (1-42); TTL = Tubulin Tyrosine Ligase; LTP = Long Term Potentiation; LTD = Long Term Depression; VASH1 = Vasohibin 1; VASH2 = Vasohibin 2; SVBP = Small Vasohibin Binding Protein; $TTL^{+/-}$ = Tubulin Tyrosine Ligase heterozygous; WT = Wild-Type; fEPSPs = field Excitatory PostSynaptic Potentials; I/O = Input/Output curves; TBS = Theta Burst Stimulation; iPSCs = induced Pluripotent Stem Cells

Introduction

The neuronal microtubule cytoskeleton plays a fundamental role in the development and long-term maintenance of axons and dendrites. Research over the past two decades has revealed that dynamic microtubules, in particular, critically contribute to synaptic structure and function within both pre- and postsynaptic compartments.[1, 2] Dynamic microtubules regulate synaptic vesicle cycling by providing paths for bidirectional transport between presynaptic terminals, a rate-limiting step in exocytosis at sites of release.[3-6] In dendritic spines, while the core cytoskeletal structure consists of actin filaments, dynamic microtubules originating in the dendritic shaft sporadically enter the spine head and directly impinge on the regulation of spine composition and morphology.[7, 8] Microtubule entry into spines is dependent on synaptic activity, Ca^{2+} influx, actin polymerization, and correlates with changes in synaptic strength.[9] In cultured rodent hippocampal neurons and organotypic slices, stimulation of postsynaptic N-methyl-D-aspartate receptors by chemical long term potentiation (LTP) protocols or glutamate photo-release leads to higher frequency and longer duration of spine invasions by microtubules, concurrent with spine enlargement.[10-12] Conversely, chemical induction of long term depression (LTD) decreases microtubule invasions, indicating that microtubules targeting into spines are sensitive to plasticity signals.[13-15] Spine invasions, as well as synaptic plasticity, specifically involve dynamic microtubules, as both invasions and LTP are blocked when microtubule dynamics are inhibited by low doses of nocodazole[11] or taxol.[8, 16] Consistent with these results, efficient contextual fear conditioning in mice appears to require transient accumulation of dynamic microtubules at dentate gyrus synapses.[17] Together, these findings indicate that changes in synaptic microtubule dynamics may affect both pre- and postsynaptic functions.

Microtubule dynamics rely on the intrinsic capacity of microtubules to alternate phases of polymerization and depolymerization. Various cellular factors have been shown to modulate microtubule dynamics including the nature of tubulin isoforms, GTP hydrolysis, microtubule associated proteins and various post-translational modifications of tubulin.[18, 19] One prominent modification is the reversible removal of the C-terminal tyrosine residue of α-tubulin subunits, which is exposed at the external surface of microtubules. This residue is cleaved off by specific tubulin carboxy-peptidases, such as the recently identified Vasohibin 1 (VASH1) - Small Vasohibin Binding Protein (SVBP) and Vasohibin 2 (VASH2)-SVBP complexes.[20-22] When detyrosinated microtubules depolymerize, the tyrosine is rapidly restored on disassembled α-

tubulin by the enzyme tubulin tyrosine ligase, thereby replenishing the soluble tubulin pool with full-length subunits that are then available for renewed polymerization.[23-27] Due to these sequential reactions, tubulin undergoes a continuous cycle of detyrosination and re-tyrosination. Detyrosinated microtubules can be further processed by cytosolic carboxypeptidases of the deglutamylase family to generate Δ2 and Δ3 tubulins through the sequential cleavage of the final 2 or 3 amino acids, respectively.[28-31] Δ2 tubulin cannot be re-tyrosinated by tubulin tyrosine ligase, and is thus removed from the tyrosination/detyrosination cycle.[27, 32] It follows that tubulin tyrosine ligase suppression induces an accumulation of detyrosinated and Δ2 -tubulins, whereas tubulin carboxypeptidase inhibition has the opposite effect.[33-35]

Newly formed tyrosinated microtubules are highly dynamic, contrary to detyrosinated microtubules which are typically more stable.[26, 36, 37] Indeed, while it is known that tubulin detyrosination can occur on previously stabilized microtubules,[38, 39] there is also evidence that detyrosination of tubulin may itself promote microtubule stability by protecting microtubules from the depolymerizing activity of kinesin-13 motors.[40] Thus, microtubule dynamics and the tyrosination/detyrosination cycle are intertwined, and modulation of the cycle is critical to processes in which microtubules need to maintain a specific dynamic state. Moreover, microtubule detyrosination confers preferential binding for specific motors and other microtubule-associated proteins, allowing tyrosination-dependent loading of selected cargoes and microtubule modulators. For example, in neurons, detyrosinated microtubules play a unique role in neuronal transport by acting as preferential tracks for kinesin-1 and kinesin-2,[41-50] while inhibiting cytoplasmic linker proteins and dynein loading onto microtubule plus ends.[33, 51] Additional roles for detyrosinated microtubules as regulators of microtubule severing enzymes have been suggested.[52, 53] In neurons, these functions regulate the trafficking of cargos, axon outgrowth and branching. For example, kinesin-1 preferentially moves along detyrosinated microtubules.[50] Kinesin-1 is involved in mitochondria trafficking,[54] targeting of α-amino-3-hydroxy-5-methyl-4-isoxazolepropionic acid (AMPA) receptors to dendrites[55] and AMPA receptor-mediated synaptic transmission.[56] Kinesin-1 may also regulate inhibitory transmission by directing the transport of gamma aminobutyric acid (GABA) receptors via huntingtin-associated protein 1.[57, 58] Furthermore, robust kinesin-2 motility requires detyrosination of α-tubulin[49] and homodimeric kinesin-2 has been implicated in the transport of glutamate receptors,

whereas disruption of kinesin-2 impaired LTP, LTD and cAMP response element-binding protein responses in mice.[59]

While the function of Δ2 tubulin remains unknown, it is very abundant in neurons where it accumulates on very long-lived microtubules.[32] Unbuffered accumulation of Δ2 tubulin, however, has been recently associated with axonal degeneration that occurs following inhibition of mitochondrial motility.[35] In the brain, significant alteration of the tyrosination/detyrosination cycle during development modifies the relative ratio of tyrosinated, detyrosinated and Δ2 tubulin, leading to severe neurodevelopmental phenotypes in mice.[34, 60] SVBP knock-out in mice, which lead to no activity of the tubulin carboxypeptidases VASH1 and VASH2, resulted in perturbed neuronal migration in the developing neocortex, microcephaly and cognitive defects, including mild hyperactivity, lower anxiety and impaired social behavior.[34] Similarly, biallelic inactivating *Svbp* variants in human cause a syndrome involving brain anomalies with microcephaly, intellectual disability and delayed gross motor and speech development.[34, 61] Finally, *tubulin tyrosine ligase* knock-out mice show disorganization of neocortical layers, disruption of the cortico-thalamic loop, and death just after birth.[60, 62] However, it remains unknown whether post-developmental alteration of the tubulin tyrosination/detyrosination cycle plays a role in neurodegenerative diseases.

Alzheimer's disease is an age-related, neurodegenerative disorder, defined by two main pathological features: overabundance of amyloid beta peptide and hyperphosphorylated tau.[63] The most prominent clinical symptom is progressive memory loss, and decreases in synaptic density are associated with cognitive impairment.[64, 65] Alzheimer's disease is a multifactorial disease, with both genetic and environmental etiologies.[66] The London (V717I) mutation in the amyloid precursor protein (APP) is sufficient to cause early onset familial Alzheimer's disease[67] and elevated amounts of oligomeric amyloid β peptide (1-42) (oAβ),[68] a variant of amyloid β peptide more likely to oligomerize[69] and to form disruptive plaques in the brain.[70]

Recently, increased levels of modified tubulin (polyglutamylated and/or Δ2) have been found in the hippocampi of postmortem patients with Alzheimer's disease, suggesting that defects in α-tubulin retyrosination may be implicated in Alzheimer's disease.[71] Interestingly, fluctuations of detyrosinated tubulin in synaptosomal fractions from the dentate gyrus and corresponding microtubule instability/stability phases have been associated with associative learning and memory consolidation.[17] In that study, aged mice failed to regulate learning-dependent

microtubule instability/stability phases and pharmacological disruption of either of the two phases led to deficits in memory formation. These data indicate that failure in regulating the tyrosination/detyrosination cycle occurs as a result of aging[17] and may play a primary role in synaptic plasticity and dementia related disorders. Moreover, oAβ induces detyrosinated microtubules in hippocampal neurons and this activity contributes to tau hyperphosphorylation and tau dependent synaptotoxicity.[72] Finally, loss of microtubule dynamics was also reported in neurons from *Kif21b* knock-out mice that exhibit learning and memory disabilities.[73] Despite these compelling evidences, whether perturbation of the tyrosination/detyrosination tubulin cycle is a molecular driver of synaptic pathology remains unexplored.

We hypothesized that loss of tubulin retyrosination and consequential accumulation of detyrosinated and Δ2 tubulins are molecular drivers of synaptic pathology by affecting microtubule dynamics in spines. Indeed, we found that in the hippocampus of tubulin tyrosine ligase hemizygous mice ($TTL^{+/-}$), reduced levels of tubulin tyrosine ligase expression led to significant changes in the tyrosinated/detyrosinated tubulin ratio and produced defects in synaptic transmission and plasticity that were associated with a loss of excitatory synapses. We examined whether tubulin tyrosine ligase depletion was a *bona fide* feature of neurodegenerative disease and found that tubulin tyrosine ligase was down-regulated in both sporadic and familial Alzheimer disease, and that abnormally high levels of detyrosinated and Δ2 tubulins accumulated in brain samples of Alzheimer's disease patients. We explored whether tubulin tyrosine ligase and dynamic microtubules had a protective effect against the loss of synapses induced by oAβ. We found that microtubule entry into spines protected neurons from spine pruning and that acute oAβ exposure decreased the fraction of spines invaded by microtubules prior to spine loss. Remarkably, tubulin tyrosine ligase expression inhibited both spine loss and the decrease in the fraction of spines invaded by microtubules, underscoring a role for retyrosinated tubulin in protecting synapses by driving dynamic microtubules into spines.

Our data unveil a role for the tyrosination/detyrosination tubulin cycle in regulating cognitive parameters such as dendritic spine density, synaptic plasticity and memory. They also provide compelling evidence for dysfunction of the cycle in Alzheimer's disease and suggest that regulation of α-tubulin retyrosination may be critical for shielding synapses against oAβ-induced synaptic injury by promoting invasion of dynamic microtubules into spines.

Materials and methods

Animals

All experiments involving mice were conducted in accordance with the policy of the Institut des Neurosciences de Grenoble (GIN) and in compliance with the French legislation and European Union Directive of 22 September 2010 (2010/63/UE). Tubulin tyrosine ligase heterozygous mice ($TTL^{+/-}$) were obtained as previously described[60] and maintained in a C57BL6 genetic background by recurrent back-crosses with C57BL6 animals from Charles River Laboratories. Th1-eYFP line H mice[74] were obtained from Jackson Labs (B6.Cg-Tgn (Thy-YFP-H) 2Jrs) and crossed with $TTL^{+/-}$ mice to generate a colony of C57BL6/Thy1-eYFP TTL mice. All experiments involving rats were approved by the Committee on the Ethics of Animal Experiments of Columbia University and performed according to Guide for the Care and Use of Laboratory Animals distributed by the National Institutes of Health. E18 pregnant Sprague Dawley rats were purchased from Charles River Laboratories.

Electrophysiology

Electrophysiological tests were done with 3 and 9-month old wild-type (WT) and $TTL^{+/-}$ mice.

Ex vivo slice preparation After cervical dislocation of the mice, brains were isolated and brain slices prepared from WT and $TTL^{+/-}$ male or female mice. The brain was removed quickly and 350 µm thick sagittal slices containing both cortex and hippocampus were cut in ice-cold sucrose solution (in mM: KCl 2.5, NaH_2PO_4 1.25, $MgSO_4$ 10, $CaCl_2$ 0.5, $NaHCO_3$ 26, Sucrose 234, and Glucose 11, saturated with 95% O_2 and 5% CO_2) with a Leica VT1200 blade microtome (Leica Microsystemes, Nanterre, France). After the cutting, the hippocampus was extracted from the slice and transferred in oxygenated artificial cerebrospinal fluid (ACSF) (in mM: NaCl 119, KCl 2.5, NaH_2PO_4 1.25, $MgSO_4$ 1.3, $CaCl_2$ 2.5, $NaHCO_3$ 26, and Glucose 11) at 37 ± 1 °C for 30 minutes and then kept at room temperature for at least 1 hour before recordings.

Electrophysiological recordings Each slice was individually transferred to a submersion-type recording chamber and continuously superfused (2 ml/minute) with oxygenated ACSF at 28°C. Extracellular recordings were obtained from the apical dendritic layers of the hippocampal CA1 area, using glass micropipettes filled with ACSF. Field excitatory postsynaptic potentials (fEPSPs) were evoked

by the electrical stimulation of Schaeffer collaterals afferent to CA1. The magnitude of the fEPSPs was determined by measuring their slope. Signals were acquired using a double EPC 10 Amplifier (HEKA Elektronik Dr. Schulze GmbH, Germany), recorded with Patchmaster software (HEKA Elektronik Dr. Schulze GmbH, Germany) and analyzed with Fitmaster software (HEKA Elektronik Dr. Schulze GmbH, Germany). Input/output (I/O) curves characterizing basal glutamatergic transmission at CA3-CA1 synapses of WT and $TTL^{+/-}$ mice were constructed by plotting mean fEPSPs slopes ± SEM as a function of stimulation intensity (10 to 100 µA). For LTP experiments test stimuli were delivered once every 15 seconds and the stimulus intensity was adjusted to produce 40-50% of the maximal response. LTP was induced using a Theta Burst Stimulation (TBS involved 5 trains with 10 bursts of 4 pulses delivered at 100 Hz, an interburst interval of 200 milliseconds and 20 second interval between each train). Average value of fEPSP slope was expressed as a percentage of the baseline response ± SEM.

Behavioral studies

Behavioral tests were done in 3 to 4-month old WT and $TTL^{+/-}$ mice. Evaluation of cognitive function was performed with spontaneous alternation in the Y maze test for working memory, and with the Novel Object Recognition test for episodic memory. Procedures were performed during the animals' light cycle. For each test, animals were habituated to the test room for 30 minutes; room lighting was set to 150 Lux and ambient sound was provided by white noise generators set for 60 dB of white noise. Animal testing order within a test was organized to prevent animals from being single housed immediately prior to being tested. Experimenter was blinded to the genotype of animals during testing. Only males were used.

Spontaneous alternation test was conducted in a Y-shaped maze, made of black Plexiglas. The maze is heightened approximately 1 meter high, constituted by 3 arms of equivalent size (L = 38 cm; W = 8 cm; H of walls = 15 cm), numbered from 1 to 3, and by equivalent angles between them (120°). The mouse was put in the center of the maze, the nose in the direction of the bottom of one of the arms. The mouse was free to explore the environment for 5 minutes. The experimenter observed the behavior by using a camera located in an independent room and noted the sequence of successive arm visits. A visit or an entrance into an arm was defined as four legs in the zone of the arm. The apparatus was cleaned with alcohol and subsequently with water between each mouse. An alternation is defined as a visit in a given arm followed by a visit into the other arm. The successive sequence of visits during 5 minutes determines the level of alternation. The performance of the animal is estimated by calculating a

percentage of alternation: Alternation index = [number of alternations/ (total number of visited zones-2)] x 100.

Novel object recognition test was performed in Y shaped maze, to about 1 meter in height, consisting of three opaque black plastic arms of equal size (L = 38 cm, W = 8 cm, H of wall = 15 cm), numbered 1 to 3, and at a 120° angle from each other. Four different objects by size, shape and pattern were used. The recognition test had three phases: habituation, familiarization and recognition. For habituation at day 1, the mouse was placed in the center of the Y-maze, without object, to freely explore the three arms for 10 minutes. For familiarization at day 2, the mouse was again placed in the center of the Y-maze which contained at each end different objects. The mouse freely explored for 5 minutes, during which it can familiarize with these three objects. For recognition test, 1 hour after familiarization, the mouse was placed in the center of the Y-maze where one object presented during the familiarization phase was replaced by a new object. The mouse freely explored for 5 minutes and the experimenter measured the time of exploration of each object using a semi-automatic key. The assessment criterion was the difference between the time of exploration of the new object and the mean time of the time of exploration of the two familiar objects. Recognition index = difference [New object – (Mean of the two familiar objects)] durations (in seconds) of exploration.

Plasmids

For lentiviral experiments, vector eGFP-pWPT (Addgene #12255, kind gift from D. Trono) was used to express eGFP, and cDNA encoding human tubulin tyrosine ligase (NP_714923, Origene #RC207805L2) was cloned in it for tubulin tyrosine ligase expression. PCR amplification and cloning of tubulin tyrosine ligase cDNA was performed with Phusion DNA polymerase (Thermo Scientific) and In-Fusion HD Cloning kit (Clontech), respectively. eGFP cDNA was removed during the cloning process to produce an untagged tubulin tyrosine ligase. For lentiviral shRNA expression, 2 tubulin tyrosine ligase shRNA sequences, cloned in pLKO.1 vector, were purchased from Sigma-Aldrich: shTTL1 (TRCN0000191515, sequence: 5' - CCG GCA TTC AGA AA GAG TAC TCA ACT CGA GTT GAC TAC TCT TTC TGA ATG CTT TTT TG - 3') and shTTL2 (TRCN0000191227, sequence: 5' - CCG GCT CAA AGA ACT ATG GGA AAT ACT CGA GTA TTT CCC ATA GTT CTT TGA GTT TTT TG - 3') [35]. The SHC001 pLKO.1-puro Empty Vector (Sigma) was used as control (shControl). For the transfection experiments, the plasmid encoding pCMV-EB3-EGFP was a kind gift from Dr. Frank Polleux. [72] Kind gifts from Dr. Erik Dent include the plasmids EB3-tdTomato (Addgene #50708) and the plasmid encoding DsRed2 (Clontech), cloned into a pCAX vector. The plasmid pEGFP-N1

with a CMV promoter was also used (Addgene #6085-1). All constructs were verified by sequencing (Eurofins and Genewiz). Plasmids were purified with HiPure Plasmid Maxiprep kits (Invitrogen).

Amyloid β peptide (1-42) oligomers preparation

Oligomer-enriched preparations of amyloid β peptide (1-42) were obtained according to previously published methods[72]. Briefly, the lyophilized amyloid β peptide (1-42) (rPeptide) was resuspended in 1,1,1,3,3,3-hexafluoro-2-propanol to a concentration of 1 mM and monomeric amyloid β peptide (1-42) aliquots were resuspended in anhydrous dimethyl sulfoxide to 5 mM followed by vortexing and 10-minute sonication. The resuspended peptide was diluted to 100 µM in ice-cold Ham's F-12 medium and incubated at 4°C for 24 hours before use.

Lentivirus production

Lentiviral particles were produced using the second-generation packaging system as previously described.[72, 75] Lentivirus encoding GFP or tubulin tyrosine ligase cDNA (packaging vectors, pWPT-based vector, Addgene, Cambridge, MA) and shTTL1, shTTL2 and control shRNA (packaging vectors pLP1, pLP2, and pLP-VSV-G, Thermofisher) were produced by co-transfection with the psPAX2 and pCMV-VSV-G helper plasmids, into HEK293T cells obtained from ATCC (ATCC-CRL-3216) using the calcium phosphate transfection method. Viral particles were collected 48 hours after transfection by ultra-speed centrifugation, prior to aliquoting and storage at -80°C.

Primary hippocampal neuronal cultures

Mouse hippocampi (E18.5) were digested in 0.25% trypsin in Hanks' balanced salt solution (HBSS, Invitrogen, France) at 37°C for 15 minutes. After manual dissociation, cells were plated at a concentration of 5,000-15,000 cells/cm^2 on 1 mg/ml poly-L-lysine-coated coverslips for fixed samples, or on ibidi glass bottom µDishes (35 mm) for live imaging. Neurons were incubated 2 hours in DMEM-10% horse serum and then changed to MACS neuro medium (Miltenyl Biotec) with B27 supplement (Invitrogen, France).

Rat hippocampi were dissected from E18 embryos, and neurons were plated on 100 µg/ml poly-d-lysine–coated 12-well plates at the density of 3×10^5 cells/well for biochemistry assays, 5×10^4 cells/dish for live imaging in the chamber of 35-mm MatTek dishes or 4×10^4 cells/coverslip on 18-mm coverslips

for fixed samples. Primary neurons were maintained in Neurobasal medium (Invitrogen) with the supplement of 2% B-27 (Invitrogen) and 0.5 mM glutamine (Invitrogen), and one third of medium was changed every 3–4 days up to 4 weeks in culture.

Lentivirus infection To perform dendritic spine quantification, 1/100 of a hippocampal cell suspension was infected by 15-minute incubation with GFP lentivirus (Lv) at a multiplicity of infection of 40. The infected population was then mixed with non-transduced cells before plating. Some of those cultures were infected at 1 day *in vitro* (DIV) with tubulin tyrosine ligase lentivirus at a multiplicity of infection of 5. Hippocampal neurons were incubated for 18 DIV at 37°C, 5% CO_2 in a humidified incubator and then fixed with 4% paraformaldehyde in 4% sucrose-containing PBS for 20 minutes. To induce acute tubulin tyrosine ligase reduction, hippocampal neurons from WT rat embryos were infected at DIV 14 or DIV 17 with lentiviral vectors containing either control or 1 of 2 independent tubulin tyrosine ligase-targeting shRNAs and incubated until DIV 21. Ectopic expression of tubulin tyrosine ligase for microtubule spine dynamics experiments was also achieved through lentiviral infection, with infection again occurring at DIV 14 and incubation until DIV 21.

Imaging of dendritic spines

For *in vivo* fixed samples, serial sections were obtained from cortical layer V of 3-month-old Thy1eYFP-H WT and Thy1eYFP-H $TTL^{+/-}$ male mice brains. Briefly, mice were anesthetized, perfused transcardially with saline followed by 4% paraformaldehyde and brain recovered. For cultured samples, hippocampal neurons from WT, $TTL^{+/-}$ and $TTL^{-/-}$ embryos were infected with eGFP containing lentivirus and fixed at DIV 18. Dendritic segments visualized by soluble eYFP and eGFP respectively, were obtained using a confocal laser scanning microscope (Zeiss, LSM 710). Serial optical sections (1024 × 1024 pixels) with pixel dimensions of 0.083 × 0.083 µm were collected at 200 nm intervals, using a × 63 oil-immersion objective (NA 1.4). The confocal stacks were then deconvolved with AutoDeblur. For *in vitro* analysis of spines in cultured hippocampal neurons isolated from rat embryos and infected with tubulin tyrosine ligase-targeting shRNAs, DiOlistic labeling using the Helios gene gun system (Bio-Rad) was performed according to the manufacturer's instructions. Tungsten particles (1.1 µm, Bio-Rad) coated with DiI (Invitrogen), which defines the neuronal architecture in red, were delivered into hippocampal neurons fixed in 4% paraformaldehyde prior to mounting with ProLong Gold antifade mounting reagent (Invitrogen). Neurons were imaged the next day using an Olympus IX8Andor Revolution XD Spinning Disk Confocal System. Z stack images were taken at 0.2 um step length for 10-15 stacks and shown as

maximum projections. Dendritic spine analysis (spine counting and shape classification) was performed on the deconvolved stacks using Neuronstudio and Neurolucida 360.[76] All spine measurements were performed in 3D from the z-stacks. The linear density was calculated by dividing the total number of spines present on assayed dendritic segments by the total length of the segments. At least 3 dendritic regions of interest were analyzed per cell from at least 3 independent cultures in each experimental condition.

Live imaging of microtubule dynamics at spines

Rat neurons grown on 35 mm glass bottom live imaging dishes (MaTek) were co-transfected with plasmids encoding either EB3-eGFP and DsRed or EB3-tdTomato and eGFP using Lipofectamine 2000 (Invitrogen). Live cell imaging was performed 24-48 hours after transfection in complete HBSS media (HBSS, 30 mM glucose, 1 mM $CaCl_2$, 1 mM $MgSO_4$, 4 mM $NaHCO_3$, and 2.5 mM HEPES, pH 7.4) using an IX83 Andor Revolution XD Spinning Disk Confocal System. The microscope was equipped with a 100×/1.49 oil UApo objective, a multi-axis stage controller (ASI MS-2000), and a controlled temperature and CO_2 incubator. Movies were acquired with an Andor iXon Ultra EMCCD camera and Andor iQ 3.6.2 live cell imaging software. Movies of microtubule dynamics at spines were acquired at 4 seconds/frame for 10 minutes with 3 z-stack planes at 0.4 um step size. Maximum projections of movies were performed by Image Math within Andor software, exported as Tiff files and analyzed in ImageJ. Kymographs were generated by drawing a region from the base of the spine to the tip of spine head. Parameters describing microtubule invading into spines were defined as follows: % of spines invaded 10 $minute^{-1}$: number of spines invaded by microtubules during 10-minute movie/total number of spines in the imaging field; invasion lifetime: total duration of EB3 residing in a spine including comet lifetimes of multiple invasions.[10] Parameters describing microtubule dynamics were defined as follows: rescue/nucleation frequency: number of rescue or nucleation events per μm^2 per minute; catastrophe frequency: number of full tracks/total duration of growth; comet density: number of comets per μm^2 per minute; growth length: comet movement length in µm; comet lifetime: duration of growth; growth rate: growth length/comet lifetime.[77]

Analysis of spine structural plasticity

Morphologies (stubby, mushroom, thin) of all protrusions invaded or not invaded by EB3 in the same imaging field before (0 hours) and after vehicle or oAβ treatment (2 hours) were individually documented using NeuronStudio Software. Percentages of the same protrusions changing to pruned,

thin, mushroom, or stubby spines were then calculated based on total number of spines invaded or not invaded by EB3 in the same field. χ^2 tests were performed on spine persistence or pruning in vehicle and oAβ treated neurons at 0 and 2 hours. χ^2 tests were also performed on spine morphology changes (to thin, to stubby, to mushroom, to pruned) in vehicle and oAβ treated neurons at 0 and 2 hours.

Biochemical analysis of post-mortem human brain tissues

Human brains were provided by the Human Brain Tissue Bank, Semmelweis University, Budapest, Hungary. Tissue samples consist of 4 regions of brain (entorhinal cortex, hippocampus, temporal and lateral prefrontal cortex) coming from a panel of 29 male and female patients aged from 52 to 93 years: 11 controls, 5, 6 and 7 from each group corresponding to Braak stadium I-II, III-IV and IV-V (Table S1).

Extraction Brain samples were homogenized 2 x 30 seconds at room temperature in (10% vol / w) 10 mM Tris, 0.32 M sucrose, pH 7.4 containing complete inhibitors cocktail (Roche) using ready to use Precellys Lysing Kit (Bertin Technologies) in a Minilys apparatus. After lysis, the homogenates were collected, frozen in liquid nitrogen and then stored at -80°C until use. When needed, frozen aliquots were diluted v/v with RIPA buffer (50 mM Tris, 150 mM NaCl, 1% NP40, 0.5% deoxycholate, 0.1% SDS, pH=8) stirred 30 minutes at 4°C and then centrifuged 10 minutes at 14000 g at 4°C. Supernatants were frozen in liquid nitrogen and then stored at -80°C until use.

Antibodies Monoclonal rat anti-tyr-tubulin (YL1/2), polyclonal anti detyrosinated, Δ2 tubulin antibodies and monoclonal anti α tubulin antibody (α3A1) were produced in the Andrieux's lab as previously described.[32] Mouse monoclonal anti-tubulin tyrosine ligase antibody ID3 was as described [78] and polyclonal antibody 13618-1-AP was purchased from Proteintech.

Western blot analysis and quantification RIPA supernatants (10 µl) were subjected to electrophoresis on stain free 4%-15% gels (Bio Rad) and then quickly transferred to Nitrocellulose using Trans-Blot Turbo Transfer System (Bio Rad). Proteins on the membrane were revealed using specific antibodies against different forms of modified tubulin (tyrosinated, detyrosinated, Δ2) and α tubulin. Anti Tyr-Tub (1/10000), anti deTyr-Tub (1/20000), anti Δ2-Tub (1/20000) and anti α tubulin (1/10000) antibodies were used with the appropriate peroxidase-/labeled secondary antibodies. Secondary antibody signal was revealed using Pierce ECL Western blotting substrate (Thermo scientific) and analyzed with ChemiDoc™MP Imaging System (Bio Rad) using Image Lab software (stain free gel

protocol) for quantification. For each lane of the blot, the software measures the integrated volume of the band corresponding to the antigen of interest. The signal is then normalized according to the total protein measured in the same lane. For every blot, one lane is dedicated to an internal standard corresponding to a WT sample (used for the entire study) and the protein-normalized signal of this standard is considered as 100%, therefore each unknown sample is calculated as a % of this standard. For each brain sample, 3 independent blots were performed and the mean intensity was calculated.

ELISA The assay was routinely performed in high binding 96-well plates (Immulon 4 HBX, Thermo Fisher). Washings throughout the assay were: 200 µl/well, three times per washing step with Phosphate Buffer Saline (PBS) buffer solution containing 0.05% Tween 20 (PBST). Anti-tubulin tyrosine ligase antibody ID3 was coated at 1/2000 in PBS (100 µl/well) overnight (~ 16 hours) at 4 °C. After washing, the plates were blocked by adding 2% Bovine Serum Albumin (BSA) in PBS (200 µl/well) for 6 h at room temperature. The plates were then washed and incubated overnight (~ 16 h) at 4 °C with tubulin tyrosine ligase standards or brain samples diluted in 1% BSA in PBS (100 µl/well). The sample diluent served as negative control. Washed plates were then incubated for 1 hour at room temperature with anti-tubulin tyrosine ligase antibody (13618-1-AP) at 1/2000 in 1% BSA in PBST (100 µl/well). Washed plates were incubated for 1 hour at room temperature with peroxidase rabbit antibody diluted 1:10000 in BSA/PBST (100 µl/well). The plates were washed and incubated with 3,3',5,5'-tetramethylbenzidine Liquid Substrate (Sigma-Aldrich) (100 µl/well). Reaction was stopped after 5 minutes by adding Stop Reagent (Sigma-Aldrich) (100 µl/well). Absorption was determined at 450 nm on Pherastar FS (BMG Labtech). For each brain sample, 3 independent ELISA were performed and the mean value was calculated. Purified tubulin tyrosine ligase was used for normalization (kind gift of M Steinmetz)[27].

Biochemical analysis of cultured primary neurons

Cortical neurons (17 DIV) isolated from mouse embryos were transduced or not with a lentivirus expressing tubulin tyrosine ligase and treated with DMSO or with 100 nM oAβ (48 h) prior to collection, washing with phosphate-buffered saline medium at 37◦C and lysis in Laemmli buffer. The protein contents of tubulin tyrosine ligase, tyrosinated and detyrosinated tubulin were analyzed by quantitative western blot with the protocol used for human brain samples as described above. Several neuronal cultures were used as indicated in figure legends and for each sample, 3 independent blots were performed.

Biochemical analysis of mouse brain tissues

Mice hippocampi were homogenized in a lysis buffer (phosphate buffer saline (PBS) without $CaCl_2$ and $MgCl_2$, 14190-094 Life Technologies) supplemented with protease (P8340, Sigma) and phosphatase inhibitor cocktails (P5726 and P0044, Sigma) at 150 mg/mL, using a Precellys apparatus homogenizer (2 x 20 seconds, 5000 rpm). Lysates were then centrifuged at 21,000 *g* for 20 minutes at 4°C. The resulting supernatants were collected and protein concentrations were determined using bicinchoninic acid assays (Pierce/Thermo Fisher Scientific). Samples were stored at −80°C until analysis.

Automated western blotting was performed with equal concentrations of protein per sample (0.125 µg/µL) using Peggy Sue™ system (Protein Simple, San Jose, CA, USA) according to the manufacturer's instructions. Detection of tyrosinated, detyrosinated tubulins and tubulin tyrosine ligase levels were assessed using appropriate primary antibodies as detailed above for human samples. Data were analyzed with Compass software (Protein Simple).

Immunohistochemical analysis of *post-mortem* brain tissues

De-identified human autopsy brain tissue was obtained from the New York Brain Bank at Columbia University (New York, NY, USA). Neuropathologically-confirmed Alzheimer's disease cases and controls were processed following published protocols.[79]

Antibodies Anti-Δ2 tubulin (AB3203) was from Millipore, anti detyrosinated tubulin (MAB5566) from Sigma Aldrich and anti tau AT8 (MN1020) from Invitrogen.

Immunolabelling brain paraffin blocks were cut into 5 µm sections and deparaffinized in xylene (7 minutes twice) followed by 95% EtOH, 90% EtOH, 80% EtOH and 70% EtOH (5 minutes each). After washing the slices in distilled H_2O 3 times, citric acid was used to retrieve antigen by boiling samples for 15 minutes. Sections were cooled for 15 minutes, washed 3 times with PBS and blocked with serum for 1 hour at room temperature prior to staining with primary antibodies (anti-detyrosinated tubulin, 1/100; anti Δ2 tubulin 1/500 and AT8 anti Tau, 1/500) at 4^{o}C overnight. The next morning sections were washed 3 times with PBS and stained with appropriate secondary antibodies (Cy3 donkey anti mouse, 1/200; Alexa 488 donkey anti rabbit, 1/200; DAPI, 1/1000) for 1 hour at room temperature. Stained samples were washed 3 times with PBS and incubated in 0.1% black Sudan in 70% EtOH for 5 minutes to

reduce auto-fluorescence of lipofuscin, rinsed with 70% EtOH until black was gone and rehydrated in distilled H_2O.

Image acquisition and analyses Coverslips were mounted with Fluoromount prior to imaging using an Oympus VS-ASW FL 2.7(Build 11032) slide scanner and Olympus soft imaging solutions camera XM10. Images were taken using a 10x objective and same exposure time was used for the same primary antibody (detyrosinated tubulin: 100 milliseconds; Δ2: 200 milliseconds; AT8 tau: 10 milliseconds; 4',6-diamidino-2-phenylindole: 10 milliseconds). The images were converted into Tiff files for analysis using MetaMorph software. Pyramidal neuron cell bodies and proximal dendrites were randomly selected in the anterior hippocampal formation and average fluorescence intensity was measured for detyrosinated and Δ2 tubulins, as well as for AT8. An average of 150 neurons were selected for each case. Pyramidal neurons were arbitrarily classified into low AT8 (1-300 A.U.), intermediate AT8 (300.01-1000 A.U.) and high AT8 (1000.01-2400 A.U.) based on AT8 staining intensity in the cell body.

Mutant APP and isogenic control iPSC cell maintenance and differentiation

Human induced pluripotent stem cells (iPSCs) in which the APPV717I (London) mutation was knocked into one allele of the control IMR90 cl.4 iPSC line (WiCell)[80-82] using CRISPR/Cas9 was generated by Dr. Andrew Sproul's lab, as has been described previously.[83]

Maintenance APPLon knockin (cl. 88) and the isogenic parent line were maintained feeder-free in StemFlex media (Life) and Cultrex substrate (Biotechne).

Neuronal differentiation bankable neural progenitors were first generated using manual rosette selection and maintained on Matrigel (Corning) as has been described previously.[83, 84] Terminal differentiations were carried out by plating 165,000 - 185,000 NPCs per 12 well plate in N2/B27 media (DMEM/F12 base) supplemented with brain-derived neurotrophic factor (20 ng/ml; Biotechne) and laminin (1 µg/ml; Biotechne) on PEI (0.1%; Sigma) / laminin (20 µg/mL)-coated plates. After 1 week of differentiation, 100 nM Cytosineβ-D-arabinofuranoside hydrochloride (Sigma) was added to reduce proliferation of remaining neural progenitors.[84] A similar strategy was used for imaging plates (MaTek Lifesciences). Differentiations were analyzed 30-40 days post plating. For later passage of neural progenitors, we employed a CD271-/CD133+/CD184+ (Biolegend) flow-cytometry purification strategy

to remove minority neural crest contaminants (CD271+) that can expand over time, as previously done.[85]

Western blot analyses of reprogrammed cortical neurons Cell lysates from WT and mutant human cortical neurons at 30-40 days of differentiation were lysed in Laemmli sample buffer and boiled at 96°C for 5 minutes. Cell lysates were sonicated by probe sonication to sheer cellular debris and genomic DNA. Proteins were separated by 10% Bis-Tris gel (Invitrogen) and transferred to nitrocellulose membrane. After blocking in 5% milk/TBS or BSA/TBS, membranes were incubated with primary antibodies (anti total tau (tau 46) (sc-32274) from Santa Cruz; anti tau AT8 (MN1020) and anti-GAPDH (MA5-15738 and PA5-85074) from Invitrogen; anti tubulin tyrosine ligase (13618-1-AP) from Proteintech; anti detyrosinated tubulin (MAB5566) from Sigma Aldrich; Anti-Δ2 antibody (AB3203) from Millipore) at 4°C overnight and 1 hour with appropriate secondary antibodies (LI-COR Biosciences). Image acquisition was performed with an Odyssey infrared imaging system (LI-COR Biosciences) and analyzed with Odyssey software.

Statistical analysis

Data analyses, statistical comparisons, and graphs were generated using GraphPad prism or the R programming language. Statistical analysis of differences between two groups was performed using Student's t tests for populations with Gaussian distribution or else with Mann Whitney's test. When comparing 3 or more univariate samples we used one-way ANOVA, except for Figures 2F, S4 and S6 in which we used the non-parametric Kruskal-Wallis test due to non-normality of the samples. When ANOVA indicated that the factor under study had a significant effect, post hoc comparisons between factor levels (using the unexplained variance calculated in the ANOVA) were performed with the Dunnett or Sidak tests, depending on whether comparisons were, respectively, with the sole control condition or between any two conditions. Post-hoc comparisons following Kruskal-Wallis test were done with the non-parametric Dunn test. For bivariate statistics we used two-way ANOVA, with type II sum of squares when samples were unbalanced (to avoid confusion between factors). Post hoc comparisons were performed between non-weighted marginal means, using Dunnett or Sidak tests, depending on whether all-vs-control or all-vs-all comparisons were needed. The calculations were performed with the R *car* and *emmeans* packages. For Fig 3B-F, as regular two-way ANOVA was not suitable we used a linear mixed model and calculation of model coefficients by restricted

maximum likelihood estimation (using the R *lmer* package). The significance of fixed effects (Braak stage and brain region) was then evaluated by Wald type II F tests (with Kenward-Roger correction) of the null hypothesis for each of the model coefficients. Post hoc comparisons were run by Sidak tests. In Fig 3H, to determine whether the distributions of immunoreactivity values in control and Alzheimer's disease neuronal populations were significantly different we used the Kolmogorov-Smirnov test. In Fig 5E, we used an overall chi-square test that showed that the proportion of pruned spines significantly depended on at least one of the two factors under study (oAβ treatment and microtubule invasion). Then to evaluate the specific association of spine resistance with microtubule entry, we calculated the odds ratio of spine pruning in vehicle versus oAβ-treated neurons, separately for microtubule-invaded and non-invaded spines. The significance of the difference between the two odds ratios was assessed with the Woolf-test of homogeneity of odds Ratios, using the R *vcd* package. In Fig S5B-C an overall chi-square test was used on two factors under study (oAβ treatment and microtubule invasion) and the 4 possible spines morphological fates. Mean differences were considered significant at $p < 0.05$ (* $p < 0.05$; ** $p < 0.01$; *** $p < 0.001$ and **** $p < 0.0001$). Some exact p values are indicated in text or figures.

Data availability

The datasets generated and/or analysed during the current study are available from the corresponding authors on request.

RESULTS

Inhibition of tubulin retyrosination induces age-dependent synaptic defects

Dynamic microtubules are crucial for synaptic plasticity and known to bear tyrosinated tubulin, and so we directly examined whether perturbation of the tubulin tyrosination/detyrosination cycle (Figure 1A) affects synaptic function. As total genetic ablation of tubulin tyrosine ligase is perinatally lethal in mice,[60] we used $TTL^{+/-}$ mice which are viable and fertile. Firstly, we confirmed that in protein extracts from hippocampi of 3 and 9-month-old $TTL^{+/-}$ mice both tubulin tyrosine ligase protein levels and tyrosinated/detyrosinated tubulin ratio were significantly reduced compared to WT mice ($TTL^{+/-}$ = -44,95 ± 3,95 % and -48.94 + 2.61 % of

WT and tyrosinated/detyrosinated tubulin ratio = -39,46 ± 5.04 % and -37.08 ± 4.71 % of WT for 3 and 9-month-old mice respectively, Figure 1B-C and Supplementary Fig. 1A-C).

We performed spontaneous alternation in Y-maze and novel object recognition memory tests (Figure 1D, E). These memory tests were selected because they broadly assess function of cognitive domains that correlate with neural circuitry disrupted early in Alzheimer's disease, including the hippocampus,[86] and have been useful to reveal memory defects in preclinical models of β-amyloidosis and tauopathy.[87, 88] $TTL^{+/-}$ mice exhibited robust deficits in spontaneous alternation in Y-Maze (20.36 ± 0.91 versus 25.50 ± 1.09 number of entries and 68.44 ± 2.13 versus 51.88 ± 2.29 % of alternation for WT and $TTL^{+/-}$ mice, respectively) (Figure 1D). Also, in the novel object recognition test, $TTL^{+/-}$ mice spent significantly less time exploring the novel object than WT mice (delta between new and familiar object of 3.17 ± 0.33 versus 1.08 ± 0.37 sec for WT and $TTL^{+/-}$ mice, respectively) (Figure 1E). $TTL^{+/-}$ mice showed no defect in locomotor activities and sensorimotor functions as well as intact hippocampus-dependent spatial memory when assessed by the Morris Water Maze Test, consistently with lack of manifested spatial navigation defects in most preclinical Alzheimer's disease models at a young age[89] (Supplementary Fig. 2). These data demonstrate that reduced tyrosinated/detyrosinated tubulin ratio impairs spatial working and short-term recognition memory with negligible effects on sensorimotor circuit development, hyperactivity and spatial navigation, a behavioral profile that is compatible with the cognitive decline observed in preclinical models of Alzheimer's disease[86-89].

Next, we investigated hippocampal synaptic transmission in 3 and 9-month-old WT and tubulin tyrosine ligase hemizygous mice. The efficacy of basal excitatory synaptic transmission was determined by field recordings of postsynaptic excitatory responses elicited by a range of electrical stimuli of axonal CA3-CA1 Schaffer collateral fibers, in hippocampal slices. While in 3-month-old animals, the input/output (I/O) curves revealed no differences between genotypes, in 9-month old mice, observed a significantly weaker postsynaptic response in $TTL^{+/-}$ than in WT animals (Figure 1F, I) indicating defective basal synaptic transmission in older $TTL^{+/-}$ mice. Furthermore, application of a theta-burst LTP protocol showed no difference in potentiation at 3-month-old mice between WT and $TTL^{+/-}$ mice (Figure 1 G-H), but a reduced potentiation in 9-month-old $TTL^{+/-}$ compared to WT mice (Figure 1 J-K, -25.04 ± 3.68 % of WT).

Altogether, these data demonstrate that a reduction in tubulin tyrosine ligase expression results in loss of tyrosinated tubulin *in vivo*, early memory defects and age-dependent hippocampal synaptic dysfunction that affects both basal transmission and activity-dependent plasticity.

Inhibition of tubulin retyrosination affects dendritic spine density

We examined the effects of tubulin tyrosine ligase reduction at the level of individual neurons by measuring dendritic spine density and morphology both *in vivo* and using neurons in primary neuronal culture. Dendritic spines are often classified in three morphological types, corresponding to successive developmental stages: thin, stubby and mushroom-like spines.[90] For *in vivo* evaluation, $TTL^{+/-}$ mice were crossed with Thy1-e-YFP-H transgenic mice to visualize dendritic spines, and spine density evaluated in layer V cortical neurons.[74] These neurons YFP levels, allowing accurate quantification of spine density (Figure 2 A), in contrast to hippocampal neurons in which expression levels were too high for proper assessment. Confocal microscopy of *in situ* cortical neurons from $TTL^{+/-}$-Thy1-eYFP-H mice showed a 15.97 ± 2.6 % decrease in dendritic spine density compared to $WT^{+/-}$-Thy1-eYFP-H littermates (2.147 ± 0.07 and 1.804 ± 0.05 spines/µm for WT and $TTL^{+/-}$, respectively). The decrease mainly affected mature forms of dendritic spines (Figure 2 A-B). A comparable drop in mature spines (-15.53 ± 1.2 % of WT) was observed in cultured hippocampal neurons obtained from $TTL^{+/-}$ embryos (1.204 ± 0.021 and 1.017 ± 0.014 spines/µm for WT and $TTL^{+/-}$, respectively, Figure 2 C-D). Similar results were obtained when acute tubulin tyrosine ligase knock-down was performed in rat hippocampal neurons using two independent tubulin tyrosine ligase-targeting shRNAs (Figure 2E, Supplementary Fig. 1D, F). Tubulin tyrosine ligase silencing resulted in an accumulation of Δ2 tubulin (Supplementary Fig. 1E, G) and induced a dramatic reduction of dendritic spine density (Figure 2E-F, -52.88 ± 2.67 %; -47.14 ± 4.30 % of WT for shRNA1, shRNA2 treated neurons respectively) with values similar to those observed in tubulin tyrosine ligase knock-out neurons (Supplementary Fig. 3, -41.17 ± 1.25 % of WT for tubulin tyrosine ligase knock-out neurons).

Together, these results show that reducing tubulin tyrosine ligase expression affects the density of dendritic spines *in vitro* and *in vivo*, providing evidence for a novel role for tubulin retyrosination in regulating structural plasticity.

Tubulin retyrosination is perturbed in Alzheimer's disease

The synaptic and behavioral defects observed when levels of tyrosinated tubulin are perturbed raised the question as to whether dysregulation of tubulin retyrosination is a feature of Alzheimer's disease, a neurodegenerative disorder in which synaptic pathology is prominent at early stages. We performed a detailed analysis of the relative amount of tubulin tyrosine ligase, tyrosinated, detyrosinated and Δ2 tubulins in postmortem human brain tissues from sporadic Alzheimer's disease patients and age-matched controls using enzymatic linked immunoassay (ELISA) and immunoblots. For these analyses, each Alzheimer's disease brain was histologically analyzed according to Braak's criteria[91] to discriminate early (Braak I-II), middle (Braak III-IV) and late Alzheimer's disease stages (Braak V-VI), as shown in Supplementary Table 1. Alzheimer's disease sequentially affects the entorhinal cortex (E), hippocampus (H), temporal cortex (T) and lateral prefrontal cortex (L). We analyzed tubulin tyrosine ligase levels and the different α-tubulin forms in protein extracts prepared from these four brain regions of Alzheimer's disease patients and controls (Figure 3A-F). Global analysis indicated a statistically significant effect of Braak stages on tubulin tyrosine ligase content (F (3, 25) = 4.3454, $*p$ = 0.0135, Figure 3B, grey box). Post-hoc comparison of tubulin tyrosine ligase content in control and Alzheimer's disease brains showed a significant decrease in temporal and lateral prefrontal cortex of Alzheimer's disease patients ($^{\#}p$ = 0.0322 and $^{\#}p$ = 0.012, respectively for Braak V-VI versus controls, Figure 3B). No significant effect of brain region on tubulin tyrosine ligase content was observed (F (3, 75) = 0.2185, p = 0.8833, Figure 3B, grey box) suggesting that the tubulin tyrosine ligase decrease observed in Alzheimer's disease samples affects the whole brain. Regarding tyrosinated tubulin levels, a global analysis indicated that there was no significant dependence on Braak stage (F (3, 25) = 1.1336, p = 0.3556, Figure 3C, grey box). For detyrosinated and Δ2 tubulin levels, the Braak stage had a global significant effect (F (3, 25) = 3.515, $*p$ = 0.0297 and F (3, 25) = 5.877, $**p$ = 0.0035 for detyrosinated and Δ2 tubulins, respectively, Figure 3D-E, grey boxes). Post-hoc comparisons in each brain region as a function of Braak stage, indicated that the detyrosinated tubulin content significantly accumulated in the hippocampus of patients with advanced disease (Figure 3D, $^{\#}p$ = 0.0131 for Braak V-VI versus controls). Further, the amount of Δ2 tubulin increased in all regions in Alzheimer's disease samples, as compared to controls (Figure 3E, $^{\#\#}p$ = 0.0018, p = 0.0584, $^{\#}p$ = 0.0195 and $\#p$ = 0.0144 for entorhinal, hippocampus, temporal and lateral cortex, respectively, for Braak V-VI

versus controls). Importantly, the amount of total tubulin did not vary with disease stage ($F(3,25) = 1.54$, $p = 0.23$, Figure 3F), confirming that the increase observed in disease samples was selective for detyrosinated and Δ2 tubulins. To note, the levels of tyrosinated, detyrosinated and Δ2 tubulins, as well as total tubulin, were significantly different among brain regions (Figure 3C-F grey boxes, (F (3, 75) = 3.1183, *p = 0.0310; F (3, 75) = 8.190, ****p= 0.00008; F (3, 75) = 10.091, ****p= 0.00001; F (3, 75) = 6.19, ****p= 0.0008 for tyrosinated, detyrosinated, Δ2 and total tubulin, respectively), a feature mostly attributable to larger concentration of tubulin in the entorhinal cortex extracts than in the other brain region samples.

Altogether, these results indicate that in Alzheimer's disease, a global tubulin tyrosine ligase impairment is present from an early stage of the neurodegeneration process and is associated with increased amounts of non-tyrosinated tubulin.

We next analyzed modifications in non-tyrosinated tubulin content *in situ* by performing an immunocytochemistry study of Alzheimer's disease brains. We performed a semi-quantitative immunofluorescence analysis of cell bodies and proximal dendrites of randomly selected individual pyramidal cells in the anterior hippocampal formation of sections from Alzheimer's disease and control tissue (Supplementary Table 2, Figure 3G-I). Each selected neuron was classified for tau pathology with either low, intermediate or high level of AT8 labelling (Ser202 and Thr205 phospho-tau antibody) and the mean intensity of detyrosinated and Δ2 tubulin staining was calculated. As expected, strongly AT8-reactive neurons were far more frequent in the Alzheimer's disease samples, consistent with the pathological scoring of control and Alzheimer's disease post-mortem human brains (Figure 3G-H, Supplementary Table 2). Interestingly, we found that Alzheimer's disease neurons with relatively low levels of phospho-tau, and thus presumably at an early stage of the degeneration process, were significantly enriched in detyrosinated and Δ2 tubulins compared to non-diseased neurons (Figure 3I, **** $p < 0.0001$ for each). In contrast, Alzheimer's disease neurons with intermediate AT8 staining still displayed significant enrichment in Δ2 tubulin compared to non-diseased neurons (Figure 3I, **** $p < 0.0001$) but a lower level of detyrosinated tubulin, presumably as a result of advanced neurodegeneration and/or accelerated conversion of detyrosinated to Δ2 tubulin in diseased brains. These *in situ* results confirmed the accumulation of non-tyrosinated tubulin in pyramidal neurons in Alzheimer's disease and indicated that it may occur at an early stage of the neurodegeneration process.

To explore whether perturbation of tubulin re-tyrosination and microtubule dynamics was a hallmark of familial Alzheimer's disease, we utilized isogenic human iPSC lines in which the Alzheimer's disease-linked London mutation (V717I) was knocked-in via CRISPR/Cas9 into one allele of the APP gene to replicate the genuine familial Alzheimer's disease genotype.[83] Human iPSCs harboring the London mutation and the isogenic control parent line were differentiated *in vitro* into human cortical neurons via a neural progenitor intermediate as previously described.[83, 84] After 30 to 40 days of differentiation, a time at which differentiated cortical neurons establish synapses, neurons were lysed, and tubulin tyrosine ligase, detyrosinated and Δ2 tubulin levels analyzed by immunoblotting. At this stage of differentiation, the mutant neurons accumulated tau protein, which was hyperphosphorylated (tau46 and AT8, Figure 4A-B), confirming the occurrence of a previously described pathological feature associated with this APP mutation.[68] Consistent with our observations of brain samples, neurons with mutant APP displayed a significant reduction in tubulin tyrosine ligase content (Figure 4C), an increase in Δ2 tubulin levels, and showed a trend in the accumulation of detyrosinated tubulin compared to isogenic controls (Figure 4D-E).

We next directly examined microtubule dynamics in human neurons by transiently expressing the microtubule plus-end binding protein, EB3-eGFP to track the dynamic behavior of microtubule plus ends (Figure 4F-L). We found that in neurons with mutant APP, while comet density, growth rate and rescue/nucleation frequency were unchanged (Figure 4G, I, L), catastrophe frequency (Figure 4H) was significantly reduced compared to WT controls with a corresponding increase in comet lifetime and length of growth (Figure 4J, K). These observations are consistent with mutant APP-dependent inhibition of microtubule dynamics by inducing resistance to undergo microtubule depolymerization.

Together, our results indicate that tubulin re-tyrosination is affected in sporadic and familial Alzheimer's disease and that inhibition of microtubule dynamics observed in mutant APP human neurons is consistent with a disrupted tubulin tyrosination/detyrosination cycle.

Tubulin retyrosination protects neurons from oAβ synaptotoxicity and promotes microtubule invasion into spines

APP variants such as the London mutant generate larger amounts of amyloid β peptide (1-42)[92] and soluble oAβ has been proposed to contribute to loss of synapses at an early stage of neurodegeneration in Alzheimer's disease.[93] We analyzed the consequences of oAβ on the behavior of spine invading

microtubules in cultured hippocampal neurons. First, we observed that neurons exposed to oAβ lost their spines in a time-dependent manner (-6.80 ± 4.63 %, -19.56 ± 4.41 %; -36.4 2 ± 2.79 % and -40.33 ± 6.57 % of control cells after 1, 2, 3 and 6 hours of oAβ exposure, respectively) (Figure 5A-B). Next, we analyzed the dynamics of microtubule invading into individual spines of neurons co-transfected with plasmids expressing EB3-eGFP and DsRed as a cell filler, in response to oAβ (Figure 5C). The dynamic parameters of spine-invading microtubules (length of growth, comet lifetime, growth rate) and spine invasion lifetime were not affected by oAβ (Supplementary Fig. 4). However, oAβ acutely inhibited microtubule entry into spines at 0.5 hours, while inducing a time-dependent renormalization of the fraction of microtubule-invaded spines starting at 2 hours (3.68 ± 0.21 %, 1.03 ± 0.29%, 5.58 ± 0.54%, 4.97 ± 0.48 % and 4.70 ± 0.77% of spines for 0, 0.5, 2, 3 and 6 hours of treatment respectively, Figure 5D), an effect possibly due to the reduction of the total number of spines over time (Figure 5B). We tracked and quantified the morphology of the same spines invaded or not invaded by microtubules in neurons treated with vehicle or oAβ for 2 hours (Figure 5E). In the absence of oAβ, microtubule-invaded thin spines appeared to switch more frequently to the larger stubby and mushroom spine types (Supplementary Fig. 5), a phenotype in agreement with previous observations reporting modifications of spine morphology upon microtubule entry.[11] However, in the presence of oAβ, spines that were not invaded by dynamic microtubules had a higher chance of being pruned (Figure 5E and Supplementary Fig. 5B-C) and the non-invaded mushroom spines that did not collapse showed increased transitions to stubby or thin spines, presumably causing additional loss of synaptic strength (Supplementary Fig. 5B-C). For example, after 2 hours of oAβ treatment, only 9 % of microtubule-invaded spines were pruned compared to 35 % of non-targeted spines (Figure 5E).

These results indicate that oAβ causes early inhibition of microtubule entry into spines, and that these changes may be functionally related to the onset of spine pruning. The renormalization of the percentage of microtubule-invaded spines that we observed at later time points might thus reflect a relative accumulation of a class of spines which are intrinsically resistant to pruning. These results further suggest that entry of dynamic microtubules, which are mainly composed of tyrosinated tubulin, may underlie the resistance of dendritic spines to synaptic injury by oAβ.

We next examined the effect of chronic exposure to oAβ on tubulin tyrosine ligase and tubulin tyrosination levels in primary cultured neurons. We found that 2 days of chronic 100 nM oAβ exposure resulted in a 25.77 ± 5.23 % reduction in tubulin tyrosine ligase content (Figure 6A), similarly to what we observed in sporadic and familial Alzheimer's disease samples (Figure 3B

and Figure 4A, C). Acute 250 nM oAβ exposure resulted in a decline of both tubulin tyrosine ligase levels and the tyrosinated/detyrosinated tubulin ratio starting at 30 minutes (Supplementary Fig. 6), a timepoint at which microtubule entry into spines was inhibited. Lentivirus-driven tubulin tyrosine ligase expression in these samples was performed to an extent that did not significantly affect tyrosinated/detyrosinated tubulin ratio nor spine density in control neurons (Figure 6A-C), and we then tested for oAβ-induced spine pruning. Strikingly, in tubulin tyrosine ligase-expressing neurons, oAβ completely failed to diminish spine density (Figure 6C-D), indicating that spine loss induced by oAβ might rely on downregulation of tubulin tyrosine ligase and tyrosinated tubulin levels. Global biochemical analysis showed that 100 nM oAβ did not appreciably alter the proportion of tyrosinated tubulin in these neurons (Figure 6B). However, it was conceivable that oAβ might have locally affected the pool of tyrosinated, dynamic microtubules available for spine entry. To explore this possibility, we set out experiments to examine whether the percentage of spines invaded by dynamic microtubules correlated with spine resistance to oAβ in neurons ectopically expressing tubulin tyrosine ligase (Figure 6E-G). We found that expression of tubulin tyrosine ligase averted the oAβ-induced drop in spine invasions by dynamic microtubules measured at 30 minutes (Figure 6F) as well as oAβ-promoted spine loss, which became detectable only 2.5 hours later (Figure 6G). To assess whether this drop in spine entries at 30 minutes could be related to the loss of tubulin tyrosine ligase and tyrosinated tubulin, we evaluated microtubule entries into spines when tubulin tyrosine ligase levels start to decrease. In hippocampal rat neurons, after 4 days of infection with shRNA against tubulin tyrosine ligase, a time point at which tubulin tyrosine ligase levels begin to drop but before spine density starts to decline, microtubule entries into spines significantly decreased (Supplementary Fig. 7A-B). Accordingly, in the TTL+/- mouse neuronal cultures, there was also a significant decrease in spine entries, as compared to the WT (Supplementary Fig. 7C).

Together, our results indicate that entry of dynamic tyrosinated microtubules into spines may underlie enhanced resistance of dendritic spines to synaptic injury and that restoring tubulin tyrosine ligase expression can protect dendritic spines from oAβ toxicity as illustrated in Figure 7.

Discussion

In this study, we identify a role for the retyrosination of α-tubulin by tubulin tyrosine ligase activity in the maintenance of synaptic function and Alzheimer disease-related synaptic dysfunction.

Our biochemical and immuno-histological analysis of $TTL^{+/-}$ mouse hippocampi confirmed that hemizygous suppression of tubulin tyrosine ligase leads to around 40% reduction of tyrosinated tubulin, and that this reduction is compatible with viability and normal life span. This result suggests that tubulin tyrosine ligase levels are rate-limiting for the maintenance of physiological amounts of tyrosinated tubulin *in vivo*.

We found that the behavioral performance of $TTL^{+/-}$ mice at 3 months revealed impairments in spontaneous alternation test and novel object recognition but no defect in spatial learning assessed by Morris Water Maze, the standard test for evaluating hippocampal-dependent memory in rodents. This behavioral profile was consistent with no alteration in hippocampal basal transmission and CA3/CA1 LTP at this early age, which was instead characterized by deficits in spatial working and intermediate-term recognition memory most likely caused by cortical circuitry dysfunction. In agreement with synaptic cortical damage at this age, we observed loss of dendritic spines in serial sections obtained from cortical layer V of 3-month-old $TTL^{+/-}$ mice. At 9 months, however, $TTL^{+/-}$ mice had a clear reduction in their basal hippocampal transmission, a defect consistent with decreased spine density observed in cultured hippocampal neurons from $TTL^{+/-}$ embryos or transiently silenced of tubulin tyrosine ligase expression. In addition, a striking decline in the LTP of synaptic strength at the Schaffer collateral synapses was observable in 9-month-old $TTL^{+/-}$ mice, demonstrating that tubulin tyrosine ligase deficiency exacerbates synaptic plasticity defects with aging.

Our in vitro analyses strongly suggest that these alterations may be related to defects in synaptic microtubule dynamics. In support of this model, we found that loss of tubulin tyrosine ligase significantly reduced the number of microtubule entries into dendritic spines and led to a significant loss of synapses. In addition, we found that entry of dynamic microtubules into spines correlated with resistance to oAβ-induced spine pruning. Strikingly, expression of tubulin tyrosine ligase in oAβ-treated neurons prevented both transient loss of microtubule entry into spines and spine pruning, indicating that restoring dynamic microtubule invasions into spines is

the mechanism by which tubulin tyrosine ligase prevents oAβ-induced loss of synapses. Matching our observed decline in tubulin tyrosine ligase and tyrosinated tubulin after 30 minutes and 3 hours of 250 nM oAβ, previous research has shown that in primary hippocampal neurons microtubules present in the dendritic shaft become less dynamic after 30 minutes of oAβ exposure and that detyrosinated tubulin levels increase by 3 hours.[72] The fine-tuning of the tyrosination-detyrosination tubulin cycle as a function of small, local cues may be important in the vicinity of synapses which are particularly dependent on entry of dynamic tyrosinated microtubules.[10, 11] Live imaging of spines invaded by microtubules during incubation with oAβ showed that the minority of spines that were invaded by microtubules during the recording period had a greater resistance to pruning than non-invaded spines. Given the pleiotropic effects that the tyrosination-detyrosination tubulin cycle plays in the regulation of neuronal transport,[45, 94-96] local re-tyrosination of tubulin by tubulin tyrosine ligase might be critical for the recruitment or removal of spine modulating cargos specifically trafficked along tyrosinated microtubules. We have observed a population of spines that are not invaded by microtubules and yet persist. There may be at least two plausible explanations for this: 1) the resistant spine lacking microtubule invasion might have been invaded prior to movie acquisition; 2) only a small fraction of spines is invaded at any given time, suggesting that not all spines have the same chance to be targeted by microtubules and/or are dependent on microtubules to avoid pruning. If not all spines are equally targeted, this would also explain why certain spines may be more resistant or particularly vulnerable to pruning.

Altogether, the electrophysiological, spine density and behavioral profile of $TTL^{+/-}$ mice shows that tubulin tyrosine ligase is required for synaptic maintenance and plasticity, and that tubulin tyrosine ligase deficiency increases synaptic vulnerability. These findings are relevant to the onset of synaptic dysfunction in neurodegenerative disease, as we find that tubulin tyrosine ligase is down-regulated in Alzheimer's disease brain, human Alzheimer's disease neurons, and primary neurons exposed to oAβ. Biochemical analysis of *postmortem* brain samples from clinically graded Alzheimer's disease patients indicated a robust loss of tubulin tyrosine ligase and a gain in detyrosinated and Δ2 tubulin compared to samples from non-affected individuals in the same age range. The correlation between disease conditions and non-tyrosinated tubulin accumulation was confirmed at the single neuron level by imaging analysis of Alzheimer's disease hippocampal sections. Deficits were narrowed to an early phase of the disease, a stage at

which neuron morphology appears normal with deficiencies mainly affecting the synaptic compartments. Our data also point out that in Alzheimer's disease the accumulation of non-tyrosinated forms of tubulin affects the whole brain, suggesting that selected circuits that go awry in Alzheimer's disease may be more vulnerable than others to loss of tubulin re-tyrosination.

The finding that the knock-in of the Alzheimer's disease-linked London mutation in APP in *in vitro* differentiated human neurons also resulted in a drop in tubulin tyrosine ligase compared to isogenic controls strongly supports a causal relationship between tubulin tyrosine ligase loss and familial Alzheimer's disease. Because the London mutation leads to an increase in the amyloidogenic processing of APP and overproduction of toxic Amyloid β species,[92] the finding suggests that tubulin tyrosine ligase down-regulation could be initiated by either defective APP processing and/or accumulation of oAβ. Indeed, chronic incubation of cultured mouse neurons with synthetic oAβ elicited a significant decline in tubulin tyrosine ligase levels, although the underlying mechanisms are yet to be defined. The altered synaptic phenotype of $TTL^{+/-}$ mice suggests that down-regulation of tubulin tyrosine ligase might in turn aggravate oAβ synaptoxicity by reducing microtubule dynamics, and thus cause further loss of synapses. This notion would be consistent with the protection against dendritic spine retraction that we observed in neurons in which tubulin tyrosine ligase was ectopically expressed.

Altogether, our results point to a modulatory role of the tyrosination/detyrosination tubulin cycle in synaptic plasticity and indicate that loss of tubulin tyrosine ligase and tubulin re-tyrosination are features of Alzheimer's disease and might be one of the mechanisms playing a pathogenic role at early stages of neurodegeneration. The results also indicate that in the early stages of Alzheimer's disease, the microtubule network appears to be less dynamic than in normal conditions, with critical loss of dynamic microtubules. They also suggest that the decrease in dynamic microtubules, rather than a global microtubule destabilization, initiates Alzheimer's disease pathology. Our pathogenesis model does not reject loss of microtubule integrity as a major pathological feature of advanced Alzheimer's disease, but rather proposes that amyloidogenic APP processing may affect synaptic function by reducing the population of dynamic microtubules entering into synapses at an early stage of the disease. While the molecular factors associated with the resistance of dynamic microtubules-invaded spines remain to be identified, our results suggest that tubulin tyrosine ligase activators may be beneficial to restore circuit integrity in sporadic and familial Alzheimer's disease. In addition, the VASH1/2-SVBP carboxypeptidases have been recently identified as a tubulin detyrosinating complexes[20, 21] suggesting

that also drugs able to modulate tubulin carboxypeptidase activity may offer a valuable new approach for therapeutic intervention in Alzheimer's disease.

Acknowledgements

We thank F. Vossier and L. Macedo for technical support; S. Andrieu, L. Romian, F. Mehr, F. Rimet, and S Bama-Toupet for animal care; Ju. Brocard for help in lentivirus preparation and E. Tein for conducting hiPSC neuronal differentiations. We are grateful to J. Crary (Icahn School of Medicine at Mount Sinai) and the Pathology Dept at CUIMC for kindly providing Alzheimer's disease and age matched control brain slices from *post-mortem* tissue. We thank M. Gagliardini and S. Jules for helping with the analysis of *post-mortem* specimens and S. Pierre-Ferrer for the characterization of lentiviral shTTL vectors in primary neuronal cultures.

Funding

Part of the work was performed at Grenoble Institut Neuroscience Photonic Imaging Center (part of the IBiSA-accredited ISdV core facility) and in CEA-IRIG animal facility (GRAL, ANR-17-EURE-0003). This work was supported by INSERM; CEA; CNRS; University Grenoble Alpes; France Alzheimer (CAPAlz-AAP SM 2018) and ANR (SPEED-Y, ANR-20-CE16-0021) grants to MJM; NIH/NIA RO3 AG060025, NIH/NIA RO1 AG050658 and NIH/NINDS R21 NS120076-01 grants to FB; RO3 AG060025 (Co-I), the Henry and Marilyn Taub Foundation, and the Thompson Foundation (TAME-AD) grants to AS. JP fellowship was from the Italian Academy at Columbia University and the Alzheimer's Association Grant AARF-20-685875; MBR postdoctoral fellowship from Ramón Areces Foundation and salaries of JMH, CC and GF from a collaborative program between Servier laboratories and AA's team.

Contributions

LP, XQ, JP, MJM, FB and AA conceived and designed the study. CB, GF, MEP, XQ, AK and JP performed molecular biology experiments and TTL lentivirus preparations. AA and MJM supervised TTL mice production, BDC and PD supervised behavioral tests and mouse brains biochemical studies. FL, FP and AB performed electrophysiological experiments. SGF performed and analyzed in vivo dendritic spine density. LP and JMH performed experiments to analyze spine density in mouse hippocampal neurons. FB, MEP and JP designed and performed the analysis of spine density in rat hippocampal neurons. JMS

and CC performed biochemical experiments with AD patient samples, JB and YG performed the associated statistical analysis. FB and XQ designed and performed in situ analysis of patient data. FB, JP, XQ and AK designed and performed analysis of microtubule entry into dendritic spines. FB, AK, JP, MBR, and AS designed and performed experiments in human cortical neurons. FB and JP designed and performed biochemical studies in rat neurons. LP, JP, YG, MJM, FB and AA wrote the manuscript, with contributions from all co-authors.

Competing interests

The authors report no competing interests.

Supplementary material

Supplementary material is available at *Brain* online.

References

1. Parato J, Bartolini F. The microtubule cytoskeleton at the synapse. *Neurosci Lett*. Mar 26 2021;753:135850. doi:10.1016/j.neulet.2021.135850
2. Waites C, Qu X, Bartolini F. The synaptic life of microtubules. *Curr Opin Neurobiol*. Apr 16 2021;69:113-123. doi:10.1016/j.conb.2021.03.004
3. Qu X, Kumar A, Blockus H, Waites C, Bartolini F. Activity-Dependent Nucleation of Dynamic Microtubules at Presynaptic Boutons Controls Neurotransmission. *Curr Biol*. Dec 16 2019;29(24):4231-4240 e5. doi:10.1016/j.cub.2019.10.049
4. Guedes-Dias P, Nirschl JJ, Abreu N, et al. Kinesin-3 Responds to Local Microtubule Dynamics to Target Synaptic Cargo Delivery to the Presynapse. *Curr Biol*. Jan 21 2019;29(2):268-282 e8. doi:10.1016/j.cub.2018.11.065
5. Guillaud L, Dimitrov D, Takahashi T. Presynaptic morphology and vesicular composition determine vesicle dynamics in mouse central synapses. *eLife*. Apr 22 2017;6doi:10.7554/eLife.24845
6. Piriya Ananda Babu L, Wang HY, Eguchi K, Guillaud L, Takahashi T. Microtubule and Actin Differentially Regulate Synaptic Vesicle Cycling to Maintain High-Frequency Neurotransmission. *The Journal of neuroscience : the official journal of the Society for Neuroscience*. Jan 2 2020;40(1):131-142. doi:10.1523/JNEUROSCI.1571-19.2019
7. Dent EW. Dynamic microtubules at the synapse. *Curr Opin Neurobiol*. Aug 2020;63:9-14. doi:10.1016/j.conb.2020.01.003
8. McVicker DP, Awe AM, Richters KE, et al. Transport of a kinesin-cargo pair along microtubules into dendritic spines undergoing synaptic plasticity. *Nature communications*. Sep 23 2016;7:12741. doi:10.1038/ncomms12741
9. Mitsuyama F, Niimi G, Kato K, et al. Redistribution of microtubules in dendrites of hippocampal CA1 neurons after tetanic stimulation during long-term potentiation. *Ital J Anat Embryol*. Jan-Mar 2008;113(1):17-27.
10. Hu X, Viesselmann C, Nam S, Merriam E, Dent EW. Activity-dependent dynamic microtubule invasion of dendritic spines. *The Journal of neuroscience : the official journal of the Society for Neuroscience*. Dec 3 2008;28(49):13094-105. doi:10.1523/JNEUROSCI.3074-08.2008
11. Jaworski J, Kapitein LC, Gouveia SM, et al. Dynamic microtubules regulate dendritic spine morphology and synaptic plasticity. *Neuron*. Jan 15 2009;61(1):85-100. doi:10.1016/j.neuron.2008.11.013
12. Schatzle P, Esteves da Silva M, Tas RP, et al. Activity-Dependent Actin Remodeling at the Base of Dendritic Spines Promotes Microtubule Entry. *Curr Biol*. Jul 9 2018;28(13):2081-2093 e6. doi:10.1016/j.cub.2018.05.004
13. Kapitein LC, Yau KW, Gouveia SM, et al. NMDA receptor activation suppresses microtubule growth and spine entry. *The Journal of neuroscience : the official journal of the Society for Neuroscience*. Jun 1 2011;31(22):8194-209. doi:10.1523/JNEUROSCI.6215-10.2011
14. Merriam EB, Lumbard DC, Viesselmann C, et al. Dynamic microtubules promote synaptic NMDA receptor-dependent spine enlargement. *PloS one*. 2011;6(11):e27688. doi:10.1371/journal.pone.0027688
15. Merriam EB, Millette M, Lumbard DC, et al. Synaptic regulation of microtubule dynamics in dendritic spines by calcium, F-actin, and drebrin. *The Journal of neuroscience : the official journal of the Society for Neuroscience*. Oct 16 2013;33(42):16471-82. doi:10.1523/JNEUROSCI.0661-13.2013
16. Shumyatsky GP, Malleret G, Shin RM, et al. stathmin, a gene enriched in the amygdala, controls both learned and innate fear. *Cell*. Nov 18 2005;123(4):697-709. doi:10.1016/j.cell.2005.08.038
17. Uchida S, Martel G, Pavlowsky A, et al. Learning-induced and stathmin-dependent changes in microtubule stability are critical for memory and disrupted in ageing. *Nature communications*. Jul 10 2014;5:4389. doi:10.1038/ncomms5389

18. Gadadhar S, Bodakuntla S, Natarajan K, Janke C. The tubulin code at a glance. *J Cell Sci*. Apr 15 2017;130(8):1347-1353. doi:10.1242/jcs.199471
19. Moutin MJ, Bosc C, Peris L, Andrieux A. Tubulin post-translational modifications control neuronal development and functions. *Developmental neurobiology*. Jul 22 2020;doi:10.1002/dneu.22774
20. Aillaud C, Bosc C, Peris L, et al. Vasohibins/SVBP are tubulin carboxypeptidases (TCPs) that regulate neuron differentiation. *Science*. Dec 15 2017;358(6369):1448-1453. doi:10.1126/science.aao4165
21. Nieuwenhuis J, Adamopoulos A, Bleijerveld OB, et al. Vasohibins encode tubulin detyrosinating activity. *Science*. Dec 15 2017;358(6369):1453-1456. doi:10.1126/science.aao5676
22. Wang N, Bosc C, Ryul Choi S, et al. Structural basis of tubulin detyrosination by the vasohibin-SVBP enzyme complex. *Nat Struct Mol Biol*. Jul 2019;26(7):571-582. doi:10.1038/s41594-019-0241-y
23. Barra HS, Rodriguez JA, Arce CA, Caputto R. A soluble preparation from rat brain that incorporates into its own proteins (14 C)arginine by a ribonuclease-sensitive system and (14 C)tyrosine by a ribonuclease-insensitive system. *J Neurochem*. Jan 1973;20(1):97-108. doi:10.1111/j.1471-4159.1973.tb12108.x
24. Baas PW, Black MM. Individual microtubules in the axon consist of domains that differ in both composition and stability. *J Cell Biol*. 1990-08-01 1990;111(2):495-509. doi:10.1083/jcb.111.2.495
25. Bre MH, Kreis TE, Karsenti E. Control of microtubule nucleation and stability in Madin-Darby canine kidney cells: the occurrence of noncentrosomal, stable detyrosinated microtubules. *J Cell Biol*. Sep 1987;105(3):1283-96. doi:10.1083/jcb.105.3.1283
26. Kreis TE. Microtubules containing detyrosinated tubulin are less dynamic. *EMBO J*. Sep 1987;6(9):2597-606.
27. Prota AE, Magiera MM, Kuijpers M, et al. Structural basis of tubulin tyrosination by tubulin tyrosine ligase. *J Cell Biol*. Feb 4 2013;200(3):259-70. doi:10.1083/jcb.201211017
28. Paturle-Lafanechere L, Edde B, Denoulet P, et al. Characterization of a major brain tubulin variant which cannot be tyrosinated. *Biochemistry*. Oct 29 1991;30(43):10523-8. doi:10.1021/bi00107a022
29. Rogowski K, van Dijk J, Magiera MM, et al. A family of protein-deglutamylating enzymes associated with neurodegeneration. *Cell*. Nov 12 2010;143(4):564-78. doi:10.1016/j.cell.2010.10.014
30. Tort O, Tanco S, Rocha C, et al. The cytosolic carboxypeptidases CCP2 and CCP3 catalyze posttranslational removal of acidic amino acids. *Mol Biol Cell*. Oct 1 2014;25(19):3017-27. doi:10.1091/mbc.E14-06-1072
31. Aillaud C, Bosc C, Saoudi Y, et al. Evidence for new C-terminally truncated variants of alpha- and beta-tubulins. *Mol Biol Cell*. Feb 15 2016;27(4):640-53. doi:10.1091/mbc.E15-03-0137
32. Paturle-Lafanechere L, Manier M, Trigault N, Pirollet F, Mazarguil H, Job D. Accumulation of delta 2-tubulin, a major tubulin variant that cannot be tyrosinated, in neuronal tissues and in stable microtubule assemblies. *J Cell Sci*. Jun 1994;107 (Pt 6):1529-43.
33. Peris L, Thery M, Faure J, et al. Tubulin tyrosination is a major factor affecting the recruitment of CAP-Gly proteins at microtubule plus ends. *J Cell Biol*. Sep 11 2006;174(6):839-49. doi:10.1083/jcb.200512058
34. Pagnamenta AT, Heemeryck P, Martin HC, et al. Defective tubulin detyrosination causes structural brain abnormalities with cognitive deficiency in humans and mice. *Hum Mol Genet*. Oct 15 2019;28(20):3391-3405. doi:10.1093/hmg/ddz186
35. Pero ME, Meregalli C, Qu X, et al. Pathogenic role of delta 2 tubulin in bortezomib-induced peripheral neuropathy. *Proc Natl Acad Sci U S A*. Jan 26 2021;118(4)doi:10.1073/pnas.2012685118
36. Webster DR, Gundersen GG, Bulinski JC, Borisy GG. Differential turnover of tyrosinated and detyrosinated microtubules. *Proc Natl Acad Sci U S A*. Dec 1987;84(24):9040-4. doi:10.1073/pnas.84.24.9040
37. Webster DR, Gundersen GG, Bulinski JC, Borisy GG. Assembly and turnover of detyrosinated tubulin in vivo. *J Cell Biol*. Jul 1987;105(1):265-76. doi:10.1083/jcb.105.1.265

38. Khawaja S, Gundersen GG, Bulinski JC. Enhanced stability of microtubules enriched in detyrosinated tubulin is not a direct function of detyrosination level. *J Cell Biol*. Jan 1988;106(1):141-9. doi:10.1083/jcb.106.1.141
39. Gundersen GG, Bulinski JC. Selective stabilization of microtubules oriented toward the direction of cell migration. *Proc Natl Acad Sci U S A*. Aug 1988;85(16):5946-50. doi:10.1073/pnas.85.16.5946
40. Peris L, Wagenbach M, Lafanechere L, et al. Motor-dependent microtubule disassembly driven by tubulin tyrosination. *J Cell Biol*. Jun 29 2009;185(7):1159-66. doi:10.1083/jcb.200902142
41. Dunn S, Morrison EE, Liverpool TB, et al. Differential trafficking of Kif5c on tyrosinated and detyrosinated microtubules in live cells. *J Cell Sci*. Apr 1 2008;121(Pt 7):1085-95. doi:10.1242/jcs.026492
42. Hammond JW, Huang CF, Kaech S, Jacobson C, Banker G, Verhey KJ. Posttranslational modifications of tubulin and the polarized transport of kinesin-1 in neurons. *Mol Biol Cell*. Feb 15 2010;21(4):572-83. doi:10.1091/mbc.E09-01-0044
43. Konishi Y, Setou M. Tubulin tyrosination navigates the kinesin-1 motor domain to axons. *Nat Neurosci*. May 2009;12(5):559-67. doi:10.1038/nn.2314
44. Guardia CM, Farias GG, Jia R, Pu J, Bonifacino JS. BORC Functions Upstream of Kinesins 1 and 3 to Coordinate Regional Movement of Lysosomes along Different Microtubule Tracks. *Cell reports*. Nov 15 2016;17(8):1950-1961. doi:10.1016/j.celrep.2016.10.062
45. Tas RP, Chazeau A, Cloin BMC, Lambers MLA, Hoogenraad CC, Kapitein LC. Differentiation between Oppositely Oriented Microtubules Controls Polarized Neuronal Transport. *Neuron*. Dec 20 2017;96(6):1264-1271 e5. doi:10.1016/j.neuron.2017.11.018
46. Kaul N, Soppina V, Verhey KJ. Effects of alpha-tubulin K40 acetylation and detyrosination on kinesin-1 motility in a purified system. *Biophys J*. Jun 17 2014;106(12):2636-43. doi:10.1016/j.bpj.2014.05.008
47. Kreitzer G, Liao G, Gundersen GG. Detyrosination of tubulin regulates the interaction of intermediate filaments with microtubules in vivo via a kinesin-dependent mechanism. *Mol Biol Cell*. Apr 1999;10(4):1105-18. doi:10.1091/mbc.10.4.1105
48. Liao G, Kreitzer G, Cook TA, Gundersen GG. A signal transduction pathway involved in microtubule-mediated cell polarization. *FASEB journal : official publication of the Federation of American Societies for Experimental Biology*. Dec 1999;13 Suppl 2:S257-60. doi:10.1096/fasebj.13.9002.s257
49. Sirajuddin M, Rice LM, Vale RD. Regulation of microtubule motors by tubulin isotypes and post-translational modifications. *Nat Cell Biol*. Apr 2014;16(4):335-44. doi:10.1038/ncb2920
50. Cai D, McEwen DP, Martens JR, Meyhofer E, Verhey KJ. Single molecule imaging reveals differences in microtubule track selection between Kinesin motors. *PLoS Biol*. Oct 2009;7(10):e1000216. doi:10.1371/journal.pbio.1000216
51. Nirschl JJ, Magiera MM, Lazarus JE, Janke C, Holzbaur EL. alpha-Tubulin Tyrosination and CLIP-170 Phosphorylation Regulate the Initiation of Dynein-Driven Transport in Neurons. *Cell reports*. Mar 22 2016;14(11):2637-52. doi:10.1016/j.celrep.2016.02.046
52. Evans KJ, Gomes ER, Reisenweber SM, Gundersen GG, Lauring BP. Linking axonal degeneration to microtubule remodeling by Spastin-mediated microtubule severing. *J Cell Biol*. Feb 14 2005;168(4):599-606. doi:10.1083/jcb.200409058
53. Roll-Mecak A, Vale RD. Structural basis of microtubule severing by the hereditary spastic paraplegia protein spastin. *Nature*. Jan 17 2008;451(7176):363-7. doi:10.1038/nature06482
54. Schwarz TL. Mitochondrial trafficking in neurons. *Cold Spring Harbor perspectives in biology*. Jun 1 2013;5(6)doi:10.1101/cshperspect.a011304
55. Setou M, Seog DH, Tanaka Y, et al. Glutamate-receptor-interacting protein GRIP1 directly steers kinesin to dendrites. *Nature*. May 2 2002;417(6884):83-7. doi:10.1038/nature743
56. Hoerndli FJ, Maxfield DA, Brockie PJ, et al. Kinesin-1 regulates synaptic strength by mediating the delivery, removal, and redistribution of AMPA receptors. *Neuron*. Dec 18 2013;80(6):1421-37. doi:10.1016/j.neuron.2013.10.050

57. Nakajima K, Yin X, Takei Y, Seog DH, Homma N, Hirokawa N. Molecular motor KIF5A is essential for GABA(A) receptor transport, and KIF5A deletion causes epilepsy. *Neuron*. Dec 6 2012;76(5):945-61. doi:10.1016/j.neuron.2012.10.012
58. Twelvetrees AE, Yuen EY, Arancibia-Carcamo IL, et al. Delivery of GABAARs to synapses is mediated by HAP1-KIF5 and disrupted by mutant huntingtin. *Neuron*. Jan 14 2010;65(1):53-65. doi:10.1016/j.neuron.2009.12.007
59. Yin X, Feng X, Takei Y, Hirokawa N. Regulation of NMDA receptor transport: a KIF17-cargo binding/releasing underlies synaptic plasticity and memory in vivo. *The Journal of neuroscience : the official journal of the Society for Neuroscience*. Apr 18 2012;32(16):5486-99. doi:10.1523/JNEUROSCI.0718-12.2012
60. Erck C, Peris L, Andrieux A, et al. A vital role of tubulin-tyrosine-ligase for neuronal organization. *Proc Natl Acad Sci U S A*. May 31 2005;102(22):7853-8. doi:10.1073/pnas.0409626102
61. Iqbal Z, Tawamie H, Ba W, et al. Loss of function of SVBP leads to autosomal recessive intellectual disability, microcephaly, ataxia, and hypotonia. *Genetics in medicine : official journal of the American College of Medical Genetics*. Aug 2019;21(8):1790-1796. doi:10.1038/s41436-018-0415-8
62. Marcos S, Moreau J, Backer S, Job D, Andrieux A, Bloch-Gallego E. Tubulin tyrosination is required for the proper organization and pathfinding of the growth cone. *PloS one*. 2009;4(4):e5405. doi:10.1371/journal.pone.0005405
63. Ittner LM, Gotz J. Amyloid-beta and tau--a toxic pas de deux in Alzheimer's disease. *Nature reviews Neuroscience*. Feb 2011;12(2):65-72. doi:10.1038/nrn2967
64. Scheff SW, Price DA, Schmitt FA, Mufson EJ. Hippocampal synaptic loss in early Alzheimer's disease and mild cognitive impairment. *Neurobiol Aging*. Oct 2006;27(10):1372-84. doi:10.1016/j.neurobiolaging.2005.09.012
65. Terry RD, Masliah E, Salmon DP, et al. Physical basis of cognitive alterations in Alzheimer's disease: synapse loss is the major correlate of cognitive impairment. *Ann Neurol*. Oct 1991;30(4):572-80. doi:10.1002/ana.410300410
66. Blennow K, de Leon MJ, Zetterberg H. Alzheimer's disease. *Lancet*. Jul 29 2006;368(9533):387-403. doi:10.1016/S0140-6736(06)69113-7
67. Tanzi RE, Hyman BT. Alzheimer's mutation. *Nature*. Apr 18 1991;350(6319):564. doi:10.1038/350564a0
68. Muratore CR, Rice HC, Srikanth P, et al. The familial Alzheimer's disease APPV717I mutation alters APP processing and Tau expression in iPSC-derived neurons. *Hum Mol Genet*. Jul 1 2014;23(13):3523-36. doi:10.1093/hmg/ddu064
69. Nirmalraj PN, List J, Battacharya S, et al. Complete aggregation pathway of amyloid beta (1-40) and (1-42) resolved on an atomically clean interface. *Science advances*. Apr 2020;6(15):eaaz6014. doi:10.1126/sciadv.aaz6014
70. Mann DM, Iwatsubo T, Ihara Y, et al. Predominant deposition of amyloid-beta 42(43) in plaques in cases of Alzheimer's disease and hereditary cerebral hemorrhage associated with mutations in the amyloid precursor protein gene. *Am J Pathol*. Apr 1996;148(4):1257-66.
71. Vu HT, Akatsu H, Hashizume Y, Setou M, Ikegami K. Increase in alpha-tubulin modifications in the neuronal processes of hippocampal neurons in both kainic acid-induced epileptic seizure and Alzheimer's disease. *Scientific reports*. Jan 9 2017;7:40205. doi:10.1038/srep40205
72. Qu X, Yuan FN, Corona C, et al. Stabilization of dynamic microtubules by mDia1 drives Tau-dependent Abeta1-42 synaptotoxicity. *J Cell Biol*. Oct 2 2017;216(10):3161-3178. doi:10.1083/jcb.201701045
73. Muhia M, Thies E, Labonte D, et al. The Kinesin KIF21B Regulates Microtubule Dynamics and Is Essential for Neuronal Morphology, Synapse Function, and Learning and Memory. *Cell reports*. May 3 2016;15(5):968-977. doi:10.1016/j.celrep.2016.03.086
74. Feng G, Mellor RH, Bernstein M, et al. Imaging neuronal subsets in transgenic mice expressing multiple spectral variants of GFP. *Neuron*. Oct 2000;28(1):41-51. doi:10.1016/s0896-6273(00)00084-2

75. Peris L, Bisbal M, Martinez-Hernandez J, et al. A key function for microtubule-associated-protein 6 in activity-dependent stabilisation of actin filaments in dendritic spines. *Nature communications*. Sep 17 2018;9(1):3775. doi:10.1038/s41467-018-05869-z
76. Rodriguez A, Ehlenberger DB, Dickstein DL, Hof PR, Wearne SL. Automated three-dimensional detection and shape classification of dendritic spines from fluorescence microscopy images. *PloS one*. Apr 23 2008;3(4):e1997. doi:10.1371/journal.pone.0001997
77. Stepanova T, Smal I, van Haren J, et al. History-dependent catastrophes regulate axonal microtubule behavior. *Curr Biol*. Jun 8 2010;20(11):1023-8. doi:10.1016/j.cub.2010.04.024
78. Wehland J, Weber K. Tubulin-tyrosine ligase has a binding site on beta-tubulin: a two-domain structure of the enzyme. *J Cell Biol*. Apr 1987;104(4):1059-67. doi:10.1083/jcb.104.4.1059
79. Vonsattel JP, Del Amaya MP, Keller CE. Twenty-first century brain banking. Processing brains for research: the Columbia University methods. *Acta neuropathologica*. May 2008;115(5):509-32. doi:10.1007/s00401-007-0311-9
80. Yu J, Vodyanik MA, Smuga-Otto K, et al. Induced pluripotent stem cell lines derived from human somatic cells. *Science*. Dec 21 2007;318(5858):1917-20. doi:10.1126/science.1151526
81. Yu J, Hu K, Smuga-Otto K, et al. Human induced pluripotent stem cells free of vector and transgene sequences. *Science*. May 8 2009;324(5928):797-801. doi:10.1126/science.1172482
82. Hu K, Yu J, Suknuntha K, et al. Efficient generation of transgene-free induced pluripotent stem cells from normal and neoplastic bone marrow and cord blood mononuclear cells. *Blood*. Apr 7 2011;117(14):e109-19. doi:10.1182/blood-2010-07-298331
83. Sun J, Carlson-Stevermer J, Das U, et al. CRISPR/Cas9 editing of APP C-terminus attenuates beta-cleavage and promotes alpha-cleavage. *Nature communications*. Jan 3 2019;10(1):53. doi:10.1038/s41467-018-07971-8
84. Topol A, Tran NN, Brennand KJ. A guide to generating and using hiPSC derived NPCs for the study of neurological diseases. *Journal of visualized experiments : JoVE*. Feb 21 2015;(96):e52495. doi:10.3791/52495
85. Cheng C, Fass DM, Folz-Donahue K, MacDonald ME, Haggarty SJ. Highly Expandable Human iPS Cell-Derived Neural Progenitor Cells (NPC) and Neurons for Central Nervous System Disease Modeling and High-Throughput Screening. *Curr Protoc Hum Genet*. Jan 11 2017;92:21 8 1-21 8 21. doi:10.1002/cphg.33
86. Miedel CJ, Patton JM, Miedel AN, Miedel ES, Levenson JM. Assessment of Spontaneous Alternation, Novel Object Recognition and Limb Clasping in Transgenic Mouse Models of Amyloid-beta and Tau Neuropathology. *Journal of visualized experiments : JoVE*. May 28 2017;(123)doi:10.3791/55523
87. Santacruz K, Lewis J, Spires T, et al. Tau suppression in a neurodegenerative mouse model improves memory function. *Science*. Jul 15 2005;309(5733):476-81. doi:10.1126/science.1113694
88. Hsiao K, Chapman P, Nilsen S, et al. Correlative memory deficits, Abeta elevation, and amyloid plaques in transgenic mice. *Science*. Oct 4 1996;274(5284):99-102. doi:10.1126/science.274.5284.99
89. Sasaguri H, Nilsson P, Hashimoto S, et al. APP mouse models for Alzheimer's disease preclinical studies. *EMBO J*. Sep 1 2017;36(17):2473-2487. doi:10.15252/embj.201797397
90. Harris KM, Weinberg RJ. Ultrastructure of synapses in the mammalian brain. *Cold Spring Harbor perspectives in biology*. May 1 2012;4(5)doi:10.1101/cshperspect.a005587
91. Braak H, Braak E. Staging of Alzheimer's disease-related neurofibrillary changes. *Neurobiol Aging*. May-Jun 1995;16(3):271-8; discussion 278-84. doi:10.1016/0197-4580(95)00021-6
92. Pahrudin Arrozi A, Shukri SNS, Wan Ngah WZ, Mohd Yusof YA, Ahmad Damanhuri MH, Makpol S. Evaluation of the Expression of Amyloid Precursor Protein and the Ratio of Secreted Amyloid Beta 42 to Amyloid Beta 40 in SH-SY5Y Cells Stably Transfected with Wild-Type, Single-Mutant and Double-Mutant Forms of the APP Gene for the Study of Alzheimer's Disease Pathology. *Appl Biochem Biotechnol*. Nov 2017;183(3):853-866. doi:10.1007/s12010-017-2468-6

93. Mroczko B, Groblewska M, Litman-Zawadzka A, Kornhuber J, Lewczuk P. Amyloid beta oligomers (AbetaOs) in Alzheimer's disease. *J Neural Transm (Vienna)*. Feb 2018;125(2):177-191. doi:10.1007/s00702-017-1820-x
94. Maeder CI, Shen K, Hoogenraad CC. Axon and dendritic trafficking. *Curr Opin Neurobiol*. Aug 2014;27:165-70. doi:10.1016/j.conb.2014.03.015
95. van den Berg R, Hoogenraad CC. Molecular motors in cargo trafficking and synapse assembly. *Adv Exp Med Biol*. 2012;970:173-96. doi:10.1007/978-3-7091-0932-8_8
96. Kapitein LC, Hoogenraad CC. Which way to go? Cytoskeletal organization and polarized transport in neurons. Research Support, Non-U.S. Gov't
Review. *Molecular and cellular neurosciences*. Jan 2011;46(1):9-20. doi:10.1016/j.mcn.2010.08.015

Figures legends

Figure 1. Tubulin tyrosine ligase reduction induces early memory defects and age-dependent alteration of synaptic plasticity. (A) Schematic representation of α-tubulin tyrosination/detyrosination cycle. TTL (tubulin tyrosine ligase), SVBP (small vasohibin-binding protein), VASH-1/2 (vasohibin-1 and -2), CCPs (cytosolic carboxypeptidases). **(B-C)** Relative amount of TTL (normalized with GAPDH) and tyrosinated/detyrosinated tubulin ratio, in protein extracts from hippocampi of 3-month-old WT and Tubulin Tyrosine Ligase heterozygous ($TTL^{+/-}$) mice. Graphs represents mean ± SEM. Mann-Whitney test, ** $p < 0.01$, **** $p < 0.0001$. $n = 10$ independent experiments for each genotype. **(D)** Spontaneous alternation in Y-maze test. Total number of arm entries and percentage of alternance of 3-month-old WT and $TTL^{+/-}$ mice. Graph represents mean ± SEM. $n = 28$ for WT and $TTL^{+/-}$ mice. Student's t test, *** $p < 0.001$, **** $p < 0.0001$. (**E**) Novel Object Recognition test. Recognition index (time spent exploring the novel object minus the time spent exploring the two familiar objects, in sec) of 3-month-old WT and $TTL^{+/-}$ mice, measured 1h after familiarization. Mean ± SEM, $n = 48$ and 40 for WT and $TTL^{+/-}$ mice, respectively. Student's t test, **** $p < 0.0001$. (**F**) Input/output (I/O) curves of 3-month-old WT and $TTL^{+/-}$ mice slices. Curves were constructed by plotting mean fEPSPs slopes ± SEM as a function of stimulation intensity. Two-way ANOVA, genotype x stimulation intensity interaction is not significant ($F(10, 80) = 0{,}3845$, $p = 0.9500$). $n = 5$ slices from 3 WT mice and $n = 5$ slices from 3 $TTL^{+/-}$ mice. **(G)** Long-Term Potentiation (LTP) of 3-month-old WT and $TTL^{+/-}$ mice. Curves represent normalized mean of fEPSPs slopes ± SEM as a function of time before and after LTP induction. Representative traces from one experiment are shown. They were extracted at the times indicated (1, 2) on the graph **(H)** Graph showing normalized mean of fEPSPs slopes ± SEM for the last 10 min of recording in WT and $TTL^{+/-}$ mice. Mann-Whitney test, ns = not significant ($p = 0.8048$). $n = 7$ slices from 3 WT mice and $n = 7$ slices from 3 $TTL^{+/-}$ mice. **(I)** Input/output (I/O) curves of 9-month-old WT and TTL +/- mice slices. Two Way ANOVA, genotype x stimulation intensity interaction ($F(10, 220) = 1{,}923$, * $p = 0.0433$). $n = 12$ slices from 5 WT mice and $n = 12$ slices from 5 $TTL^{+/-}$ mice. **(J)** Long-Term Potentiation (LTP) of 9-month-old WT and $TTL^{+/-}$ mice. Representative traces from one experiment are shown. They were extracted at the times indicated (1, 2) on the graph. **(K)** Graph showing normalized mean of fEPSPs slopes ± SEM for the last 10 minutes of recording in WT and $TTL^{+/-}$ mice. Mann-Whitney test, ** $p = 0.0021$; $n = 10$ slices from 4 WT mice and $n = 10$ slices from 4 $TTL^{+/-}$ mice.

Figure 2. Tubulin tyrosine ligase reduction decreases dendritic spine density *in vivo* and in cultured neurons. **(A)** Confocal images showing representative examples of dendritic segments of cortical neurons from 4-month-old Thy1-eYFP-H WT and Thy1-eYFP-H tubulin tyrosine ligase heterozygous ($TTL^{+/-)}$ mice. **(B)** Total dendritic spine density, or that of each different morphological type of spines, is represented for Thy1-eYFP-H WT and Thy1-eYFP-H $TTL^{+/-}$ cortical neurons. Graphs represent mean ± SEM. *n* = 36 neurons from 4 independent animals of each genotype. Student's t test, * $p < 0.05$; *** $p < 0.001$ and ns = not significant. **(C)** Confocal images showing representative examples of the dendritic segments of GFP-expressing WT and $TTL^{+/-}$ hippocampal neurons in culture at 17 DIV. **(D)** Total dendritic spine density, or that of each different morphological types of spines are represented for WT and $TTL^{+/-}$ hippocampal cultured neurons. Graphs represent mean ± SEM. *n* = 27 and 34 neurons from WT and $TTL^{+/-}$ embryos from at least 3 independent cultures. Student's t test, * $p < 0.05$; ** $p < 0.01$; **** $p < 0.0001$ and ns = not significant. **(E)** Confocal images showing representative examples of dendritic segments of DiOilistic labeled WT rat hippocampal neurons in culture at 21 DIV, infected with control shRNA or shRNA targeting tubulin tyrosine ligase (shTTL1 and shTTL2). **(F)** Total dendritic spine density or that of each different morphological types of spines, of hippocampal neurons infected with control shRNA (non-coding shRNA) or 2 independent shRNA lentiviruses targeting tubulin tyrosine ligase (shTTL1 and shTTL2). Graphs represent mean ± SEM. *n* = 71, 124 and 60 neurons from control shRNA, shTTL1 and shTTL2 respectively, from at least 3 independent cultures. Kruskal-Wallis with Dunn's multi-comparison test, * $p < 0.05$; ** $p < 0.01$; **** $p < 0.0001$ and ns = not significant. Spines assignation to thin, stubby or mushroom categories was performed according to morphological parameters described in Figure S5.

Figure 3. Loss of tubulin tyrosine ligase and increased non-tyrosinated tubulin levels in sporadic Alzheimer's disease brain samples. **(A)** Representative immunoblot analysis of tyrosinated, detyrosinated, Δ2 and α tubulin levels in brain homogenates from entorhinal cortex (E), hippocampus (H), temporal (T) and lateral prefrontal cortex (L) from control, early Alzheimer's disease (Braak I-II), middle Alzheimer's disease (Braak III-IV) and late Alzheimer's disease (Braak V-VI) patients. In each blot an internal standard corresponding to a WT sample was used for normalization and considered as 100% and the values for each unknown sample was calculated as a % of this standard (see material and methods). **(B-F)** Quantification of tubulin tyrosine ligase (TTL) protein expression, modified tubulins (tyrosinated, detyrosinated and Δ2 tubulin) and α tubulin levels in each brain region from control and Alzheimer's disease patients. Graphs represent mean ± SEM. The dependence of protein levels on, respectively, clinical stage and brain area was quantitated in each case using a linear mixed model, with

Braak stage and brain region as fixed effect factors. Boxed p values measure the overall significance of these factors (type II Wald F test of model coefficients). In each brain area, post-hoc testing of variations due to individual Braak stages was performed by Dunnett's test of differences with control. Significance levels are indicated as follows: $^{\#}$ $p < 0.05$ and $^{\#\#}$ $p < 0.01$. n = 11, 5, 6, and 7 for Control, Braak I-II, Braak III-IV and Braak V-VI Alzheimer's disease patient brains, respectively. Each sample was analyzed in triplicate. (**G**) Representative images of detyrosinated, Δ2 tubulin and phospho-tau in pyramidal neurons of hippocampi from Alzheimer's disease patients. Dual immunostaining of detyrosinated (upper panel) or Δ2 tubulin (lower panel) and AT8-reactive phospho-tau, combined with nuclear staining with DAPI, was performed on sections of control and Alzheimer's disease patient hippocampi. Neurons with low (white arrowheads), intermediate (white arrows) or high (red arrows) levels of AT8 immunofluorescence are shown. Scale bar: 50 µm. (**H**) Relative frequency distribution of phospho-tau (AT8) immunofluorescence levels (arbitrary units) in pyramidal neurons of control and AD brains. Low, intermediate, and high phospho-tau groups were defined based on fluorescence intensity. Two-sample Kolmogorov-Smirnov test, **** $p < 0.0001$. (**I**) Intensity of detyrosinated tubulin (left graph) or Δ2 tubulin (right graph) immunofluorescence in pyramidal cell bodies of Alzheimer's disease hippocampal neurons relative to control, shown as a function of AT8 labelling level. Mean ± SEM. For detyrosinated tubulin, n = 382 and 67 neurons in controls and n = 296 and 162 for Alzheimer's disease neurons in low and intermediate phospho-tau groups, respectively. For Δ2 tubulin, n = 249 and 45 neurons in controls and n = 91 and 133 for Alzheimer's disease neurons in low and intermediate phospho-tau groups, respectively. Mann-Whitney test, **** $p < 0.0001$.

Figure 4. Loss of tubulin tyrosine ligase and increased non-tyrosinated tubulin levels correlate with inhibition of microtubule dynamics in human cortical APP-London neurons. **(A)** Immunoblot analysis of phospho-specific tau (AT8), total tau (tau46), tubulin tyrosine ligase (TTL), detyrosinated tubulin and Δ2 tubulin of tubulin tyrosine ligase from lysates of human cortical neurons, derived from WT and APP London (V717I) knocked-in iPSCs isogenic lines. GAPDH was used for tau and TTL normalization and total tubulin for modified tubulins. Immunoblot quantifications of phospho-tau normalized to total tau **(B)**, tubulin tyrosine ligase (TTL) **(C)**, detyrosinated **(D)** and Δ2 tubulin **(E).** Data are expressed as a ratio of WT and graphs represent mean ± SEM. Data are expressed as a ratio of WT and graphs represent mean ± SEM. n = 5, 5, 4 and 4 independent neuronal differentiation experiments for B, C, D and E respectively. Mann Whitney test, ns = not significant, * $p < 0.05$, ** p<0.01. **(F)** WT and APP-London human cortical neurons expressing EB3-GFP. Representative neurites (dashed boxes) from human cortical neurons were analyzed for microtubule dynamics and kymographs of these regions are shown below. Scale bar: 10

µm. (**G-L**) Parameters of microtubule dynamics are represented as mean ± SEM. *n* = 14 neurites from WT and APP-London neurons for **G** to **I**, and n = 44 comets for **J**, 42 comets for **K** and 38 comets for **L**, from WT and APP-London neurons respectively. Student's t-test, ns = not significant, ** $p < 0.01$ and *** $p < 0.001$.

Figure 5. Acute oAβ treatment affects spine invasion by dynamic microtubules in neurons. (A) Confocal images showing representative examples of dendritic segments of eGFP expressing WT rat hippocampal neurons (17 DIV) treated with DMSO or with 250 nM of oligomeric amyloid β peptide (1-42) (oAβ) for 2 days. (**B**) Graphs of the percentage of dendritic spine density in WT cultured neurons incubated with oAβ over 6 hours. Data are expressed as a % of baseline and graphs represent mean ± SEM. *n* = 4 neurons analyzed over time. One-way ANOVA with Dunnett's multiple comparison test, * $p < 0.05$ and *** $p < 0.001$. (**C**) Representative stills from videos of a WT neuron (21 DIV) transfected with DsRed and EB3-eGFP to visualize dendritic spines and the growing plus ends of microtubule, before and 2 hours after oAβ treatment. Spines that will prune are highlighted with a green arrow at time 0, and with an empty green arrow after 2 hours of oAβ treatment. The spine that will be invaded by a microtubule is highlighted with a blue arrow at time 0 and persists after 2 hours of oAβ treatment. Microtubule invasion into the spine is highlighted with a red arrow. Spines that are not invaded but persist after oAβ treatment are highlighted with arrows in magenta (**D**) Percentage of spines invaded by microtubules before and after oAβ exposure at the indicated times. Graphs represent mean ± SEM. *n* = 22, 10, 9, 6 and 5 neurons at each time point. One-way ANOVA with Dunnett's multiple comparison test, ns = not significant, ** $p < 0.01$ and **** $p < 0.0001$. Number of spines: 402, 150, 411, 191, 321, 342 and 285 for control and Aβ (0.5h, 1h, 1.5h, 2h, 3h and 6h) conditions, respectively) (**E**) Total percentage of spine pruning or resistance to vehicle or oAβ incubation. Graph represents the mean percentage of non-invaded spines (left) or microtubule-invaded spine fate (right) for either fate. Spines invaded by microtubules (n = 45 and 24) and spines non-invaded by microtubules (n = 43 and 43) for vehicle and oAβ conditions, respectively. Microtubule-invaded spines were significantly more resistant to oAβ-induced pruning than non-invaded spines (overall dependence of the spine pruning rate on microtubule invasions and oAβ treatment: $X^2 = 43.64$, 4 df, **** $p < 0.0001$, chi-square test; odds-ratio of resistance to oAβ in microtubule -invaded vs; non-invaded spines (1.15 vs. 5.44, $X^2 = 5.27$, 1df, * p= 0.021, Woolf -test).

Figure 6. Ectopic tubulin tyrosine ligase expression rescues neurons from oAβ-induced dendritic spine loss and resumes microtubule invasions into spines. (**A-B**) Immunoblot analysis of tubulin tyrosine ligase (TTL) (**A**) and tyrosinated/detyrosinated tubulin ratio (**B**) from WT mouse cortical neurons (17 DIV) transduced or not with a lentivirus expressing TTL and chronically treated with DMSO or with 100 nM oAβ. Data are expressed as a % of WT and graphs represent mean ± SEM. (**A**) *n* = 8, 7, 4 and 4 cultures for WT, WT+ Aβ, WT+TTL and WT+Aβ+TTL respectively. Two Way ANOVA, oAβ treatment x TTL expression interaction (*F* (1, 19) = 14.6, ** *p* = 0.0012). All values were compared to WT, Dunnett's multiple comparison test, * *p*<0.05 and **** *p*<0.0001. (**B**) *n* = 5, 5, 3 and 3 cultures for WT, WT+ oAβ, WT+TTL and WT+oAβ+TTL respectively. Two Way ANOVA, oAβ treatment x TTL expression interaction (*F* (1, 12) = 1.309, *p* = 0.274). All values were compared to WT, Dunnett's multiple comparison test, ns = not significant. (**C**) Graphs of total dendritic spine density in cultured WT neurons treated as in A. Graphs represent mean ± SEM. *n* = 27, 26, 20 and 20 neurons for WT, WT+ oAβ, WT+TTL and WT+oAβ+TTL respectively. Two Way ANOVA, oAβ treatment x TTL expression interaction (*F* (1, 89) = 58.44, **** *p* < 0.0001). All values were compared to WT, Dunnett's multiple comparison test, ns = not significant and **** *p*<0.0001. (**D**) Confocal images showing representative examples of dendritic segments of GFP-expressing WT hippocampal mouse neurons (17 DIV) chronically treated with DMSO or with 100 nM oAβ. (**E**) Representative stills from videos of rat WT neurons (18 to 21 DIV) transduced or not with a TTL containing lentivirus and transfected with plasmids encoding eGFP and EB3-tdTomato to visualize the dendrites and spines and the growing plus ends of microtubule, respectively. Cells were incubated with vehicle or with 250 nM of oAβ for 30 minutes. Microtubule invasions of spines are highlighted with a red arrow. (**F**) Percentage of spines invaded by microtubules after vehicle or oAβ exposure. Graphs represent mean ± SEM. *n* = 9 neurons for each condition. Two Way ANOVA, oAβ treatment x TTL expression interaction (*F* (1, 32) = 4.76, p = 0.037). Holm-Sidak's multiple comparison test, ns = not significant, * *p* < 0.05. (**G**) Graphs of total dendritic spine density in cultured neurons treated as in E and incubated with vehicle or with oAβ for 30 minutes or 3 hours. Graphs represent mean ± SEM. *n* = 6 neurons of each condition. Two-way ANOVA, oAβ treatment x TTL expression interaction (*F* (2, 30) = 7.11, p = 0.003). Holm-Sidak's multiple comparison test, ns = not significant, **** *p* < 0.0001. For F ang G, number of spines analyzed: n = 119, 117, 106, 123, 75 and 106 for control, control + TTL, control + Aβ 30 min, control +TTL + Aβ 30 min, control + Aβ 3 hours and control + TTL + Aβ 3 hours, respectively.

Figure 7. Schematic representation of tubulin tyrosine ligase, of modified tubulins in dendritic shafts and dendritic spines and of spine density in neurons (normal conditions and under oAβ exposure). Tyrosinated tubulin dimers polymerize into dynamic tyrosinated microtubules (red). Tubulin

carboxypeptidases (VASH-SVP) detyrosinate long lived microtubules (green). After depolymerization, tubulin tyrosine ligase (in grey) retyrosinates tubulin dimers. Very stable detyrosinated microtubules are substrate of cytosolic carboxypeptidases (CCPs) to form $\Delta 2$ microtubules (blue) that exits the tyrosination/ detyrosination cycle.

In mature neurons from control patients (or wild type mice), tyrosinated microtubules form a shell at the outer part of the dendrite while detyrosinated and Δ2 microtubules localize to the inner part. Some dynamic microtubules from the dendrite transiently invade dendritic spines.

In neuronal models of Alzheimer's disease, Aβ oligomers exposure have a sequential effect on microtubule behavior and dendritic spine retraction: short time incubation with Aβ oligomers induces a decrease in TTL content, an accumulation of detyrosinated and Δ2 microtubules, a decrease in the frequency of microtubule invasion into spines with no change in dendritic spine density; longer incubation accentuates this phenotype and induces spine retraction.

Ectopically controlled TTL expression restores tyrosinated, detyrosinated and Δ2 tubulin balance, microtubule invasion into the spines and dendritic spine density.

Figure 1

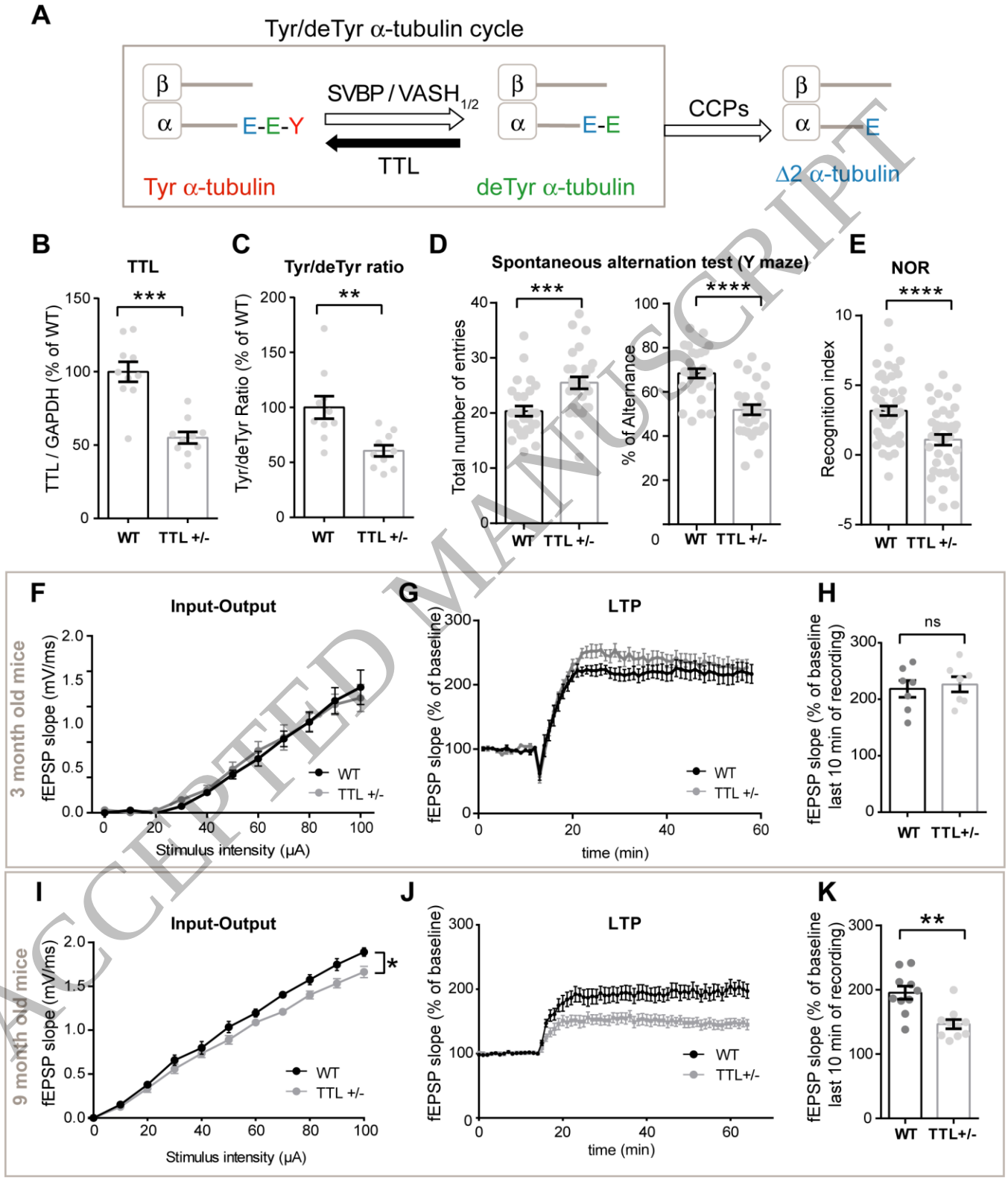

Figure 1
182x224 mm (5.4 x DPI)

Figure 2

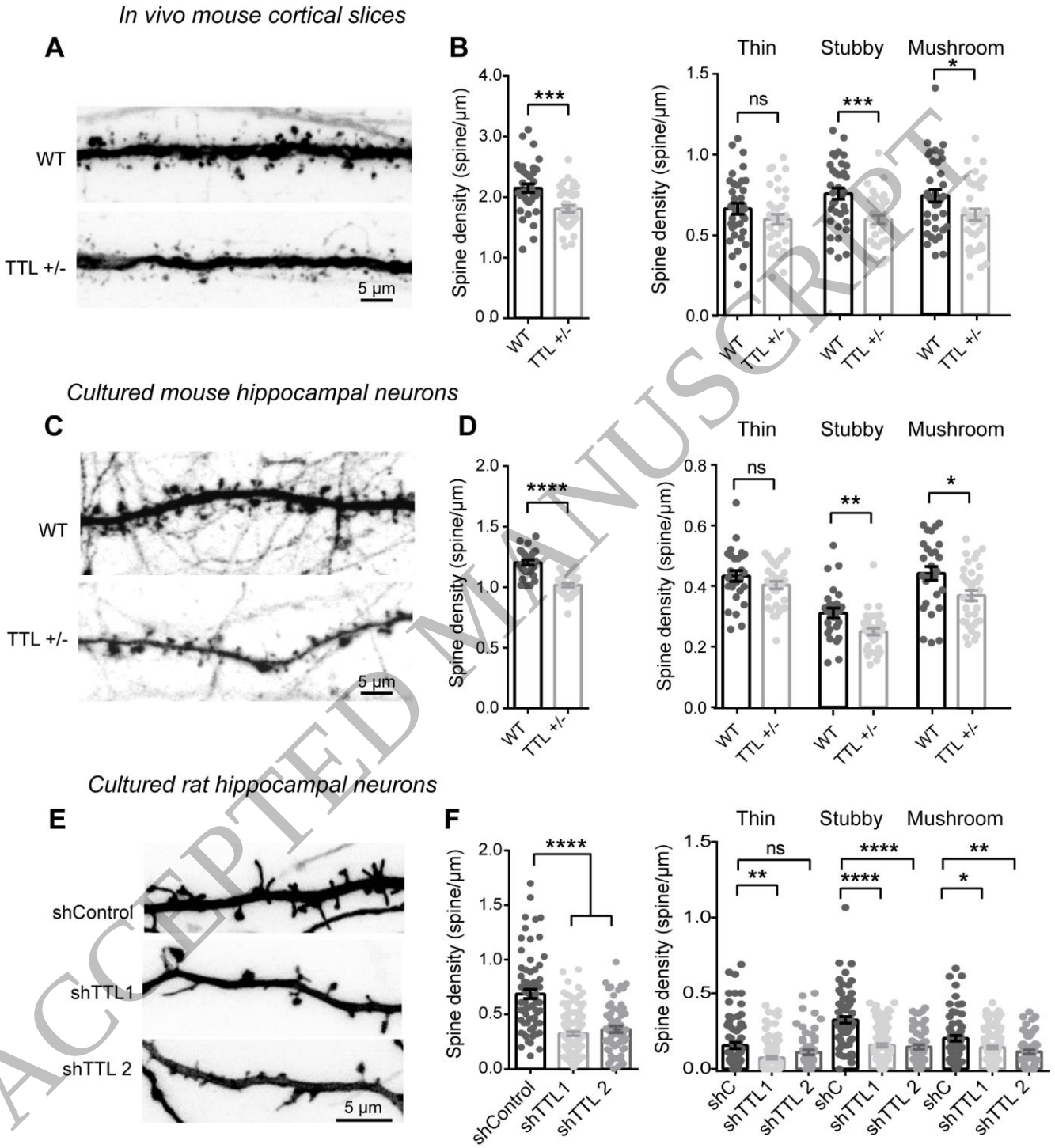

Figure 2
175x199 mm (5.4 x DPI)

Figure 3

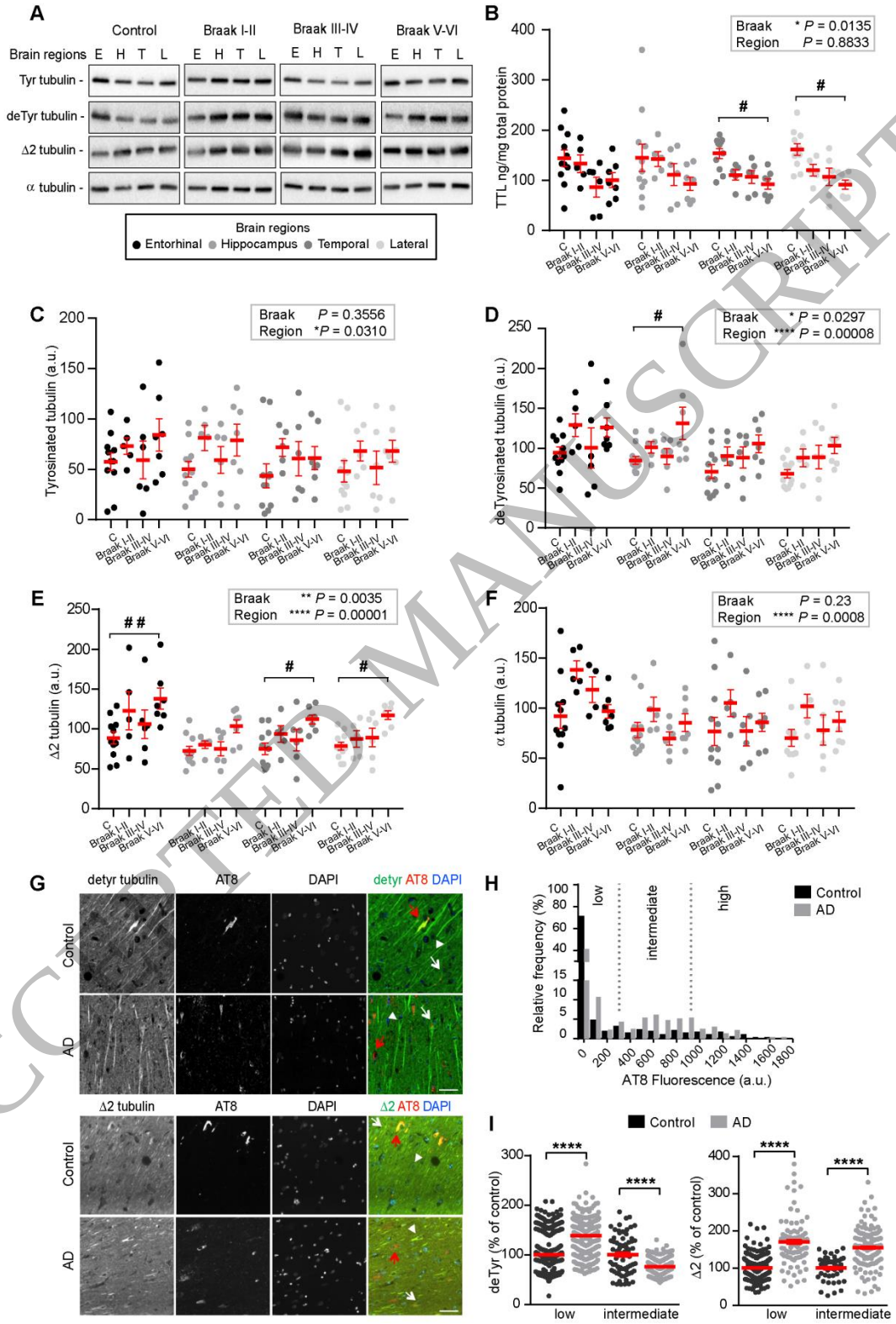

Figure 3
182x281 mm (5.4 x DPI)

Figure 4

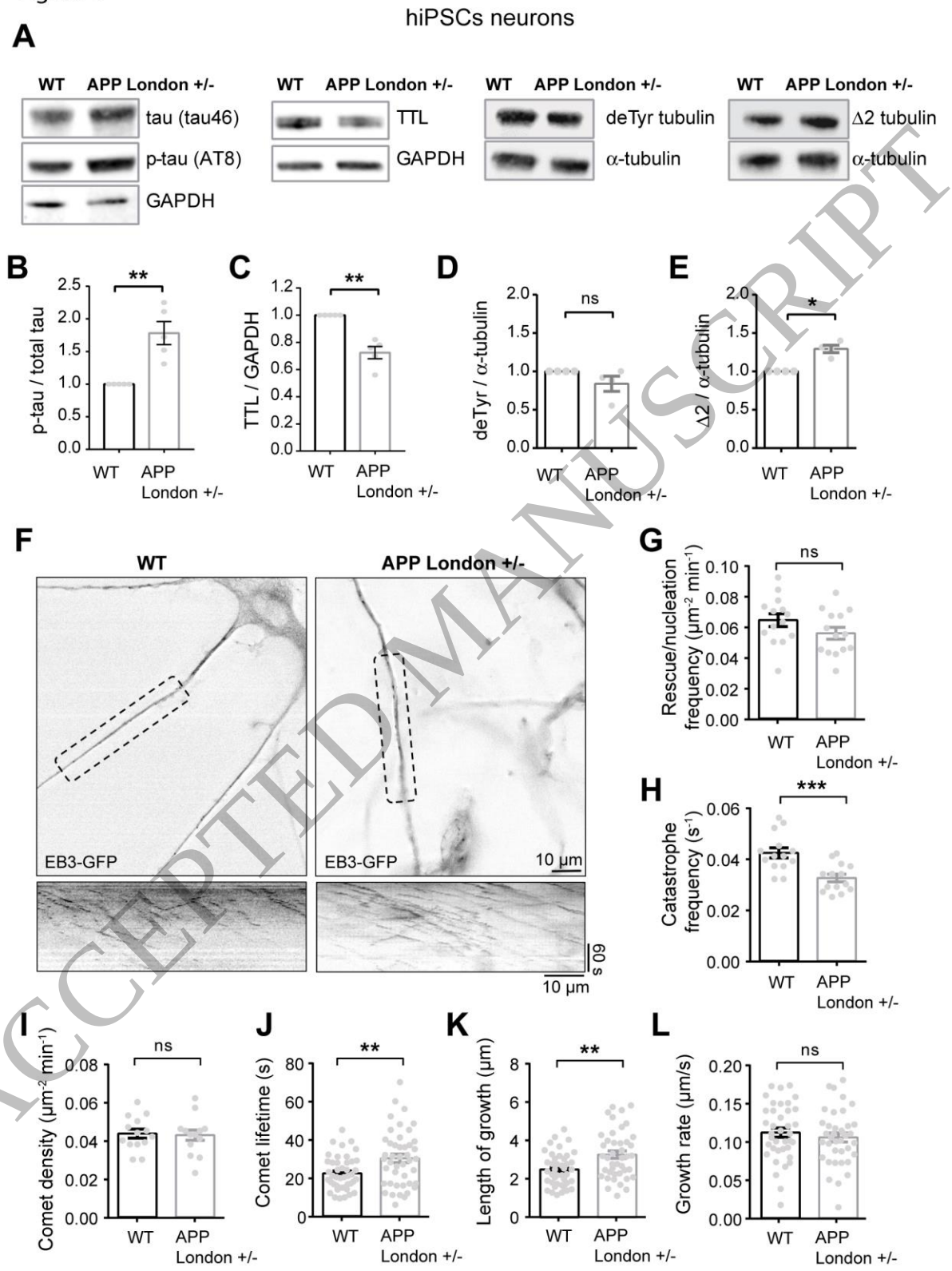

Figure 4
154x214 mm (5.4 x DPI)

Figure 5

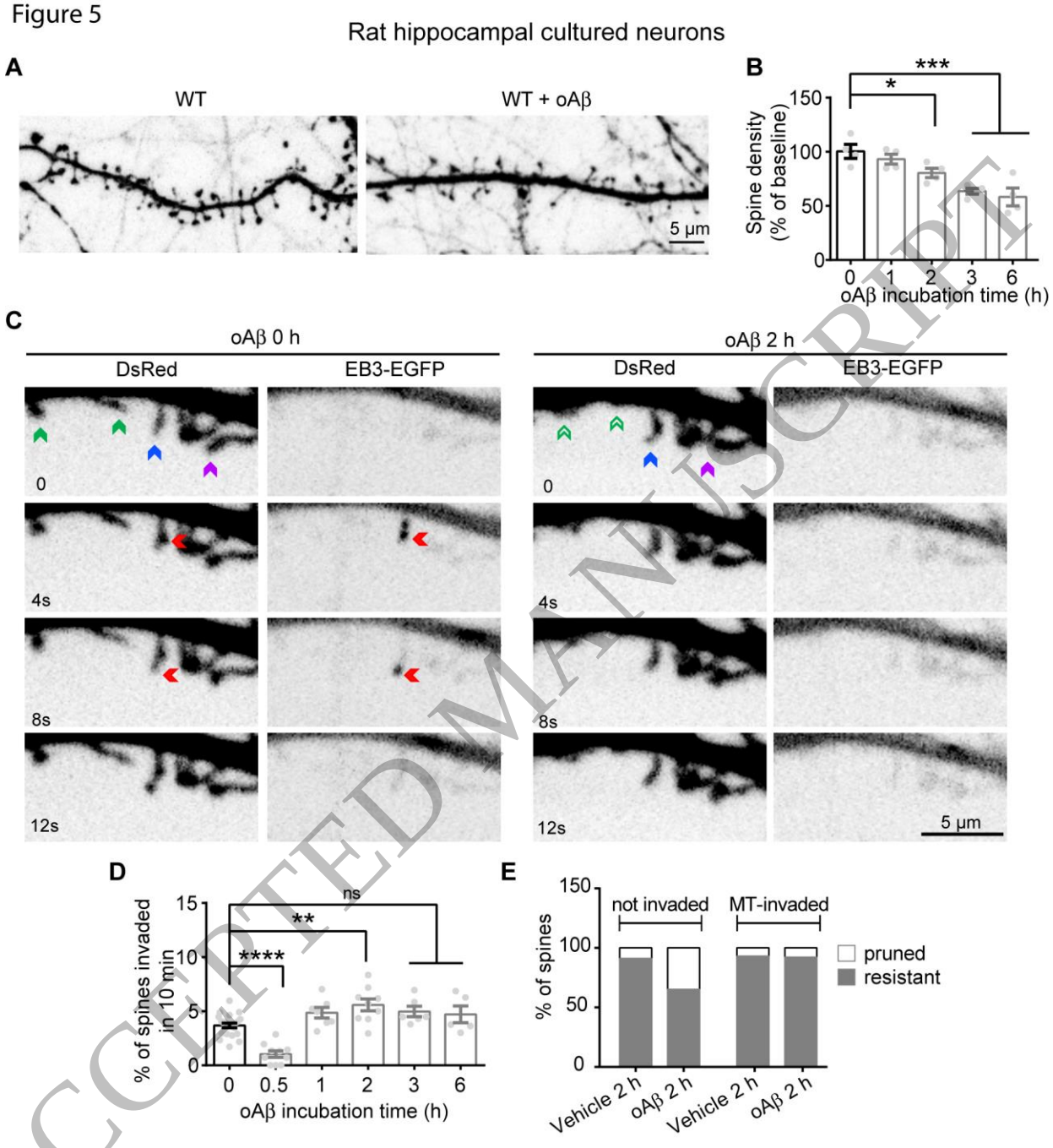

Figure 5
163x179 mm (5.4 x DPI)

Figure 6

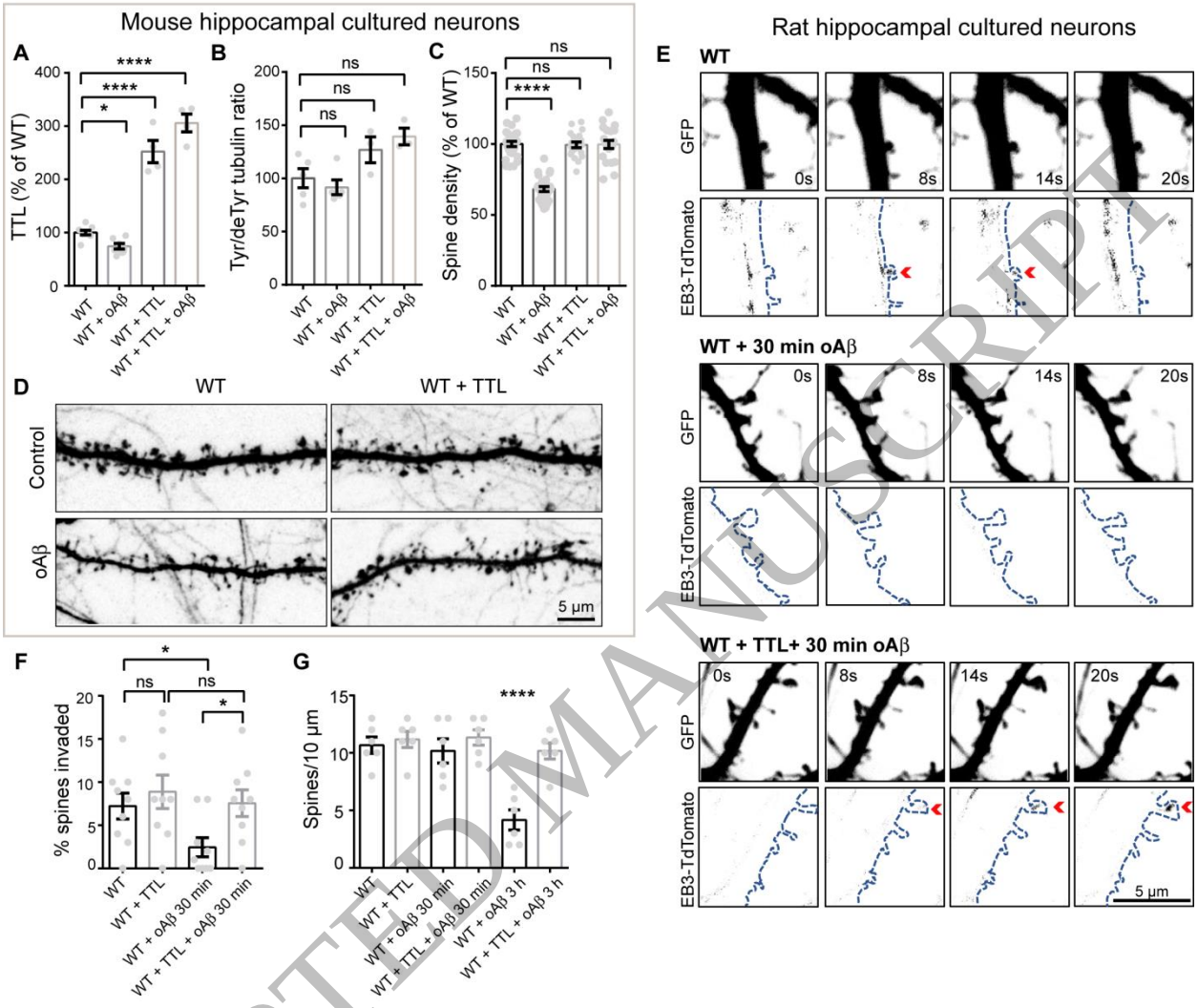

Figure 6
193x168 mm (5.4 x DPI)

Figure 7

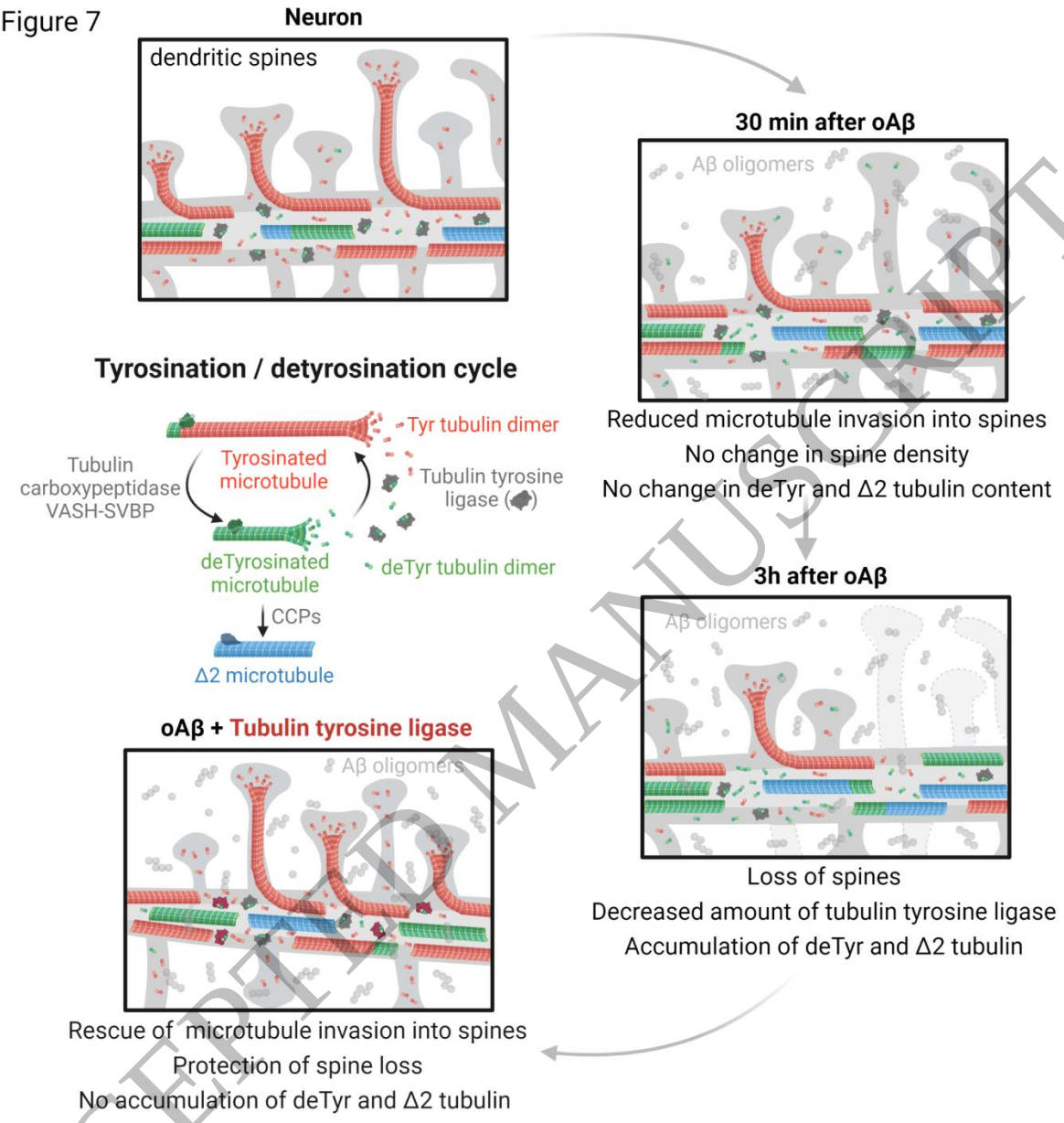

Figure 7
200x200 mm (5.4 x DPI)